

Static and Fatigue Testing of Mechanical Life Extension Options for Plates Containing Elongated Holes

R. L. Evans and M. Heller

DSTO-TR-1202

DISTRIBUTION STATEMENT A:
Approved for Public Release -
Distribution Unlimited

20020226 085

Static and Fatigue Testing of Mechanical Life Extension Options for Plates Containing Elongated Holes

R. L. Evans and M. Heller

**Airframes and Engines Division
Aeronautical and Maritime Research Laboratory**

DSTO-TR-1202

ABSTRACT

F-111 representative static and fatigue testing has been undertaken to assess the suitability of AMRL designed stress-bridge and interference-fit plug options for the fatigue life enhancement of plates containing non-circular elongated holes of 2:1 aspect ratio. For the stress-bridge design, an improvement in strain concentration factor of 38% was demonstrated for lower magnitude remote loads as compared to plates with unenhanced holes. Conversely, during typical high loads, the alternating strain range was negligibly improved due to slipping of the feet. Hence during the fatigue tests there was extensive specimen cracking. However, excellent results were achieved with the interference-fit plug design, where the peak elastic strain concentration factor was reduced by 79% as compared to the unenhanced case. This design also prevented the introduction of detrimental residual tensile stresses during high loads. Consequently, for these enhanced specimens, crack growth during fatigue testing was completely prevented, and very large extensions in fatigue lives were demonstrated. Thus the interference-fit plug is considered a very suitable option for the fatigue life extension of elongated holes such as the critical fuel flow vent holes in the F-111 wing pivot fitting.

RELEASE LIMITATION

Approved for public release

DEPARTMENT OF DEFENCE **DSTO**
DEFENCE SCIENCE & TECHNOLOGY ORGANISATION

AQ F02-05-0914

Published by

*DSTO Aeronautical and Maritime Research Laboratory
506 Lorimer St
Fishermans Bend Vic 3207 Australia*

Telephone: (03) 9626 7000

Fax: (03) 9626 7999

© Commonwealth of Australia 2001

AR-012-007

August 2001

APPROVED FOR PUBLIC RELEASE

Static and Fatigue Testing of Mechanical Life Extension Options for Plates Containing Elongated Holes

Executive Summary

An area of major concern for the F-111 airframe currently in service with the Royal Australian Air Force (RAAF) is the wing pivot fitting (WPF). Fatigue cracking in service and structural failure during cold proof load tests has occurred in this primary structural component. Some of the main locations of cracking are the machined non-circular fuel flow vent holes (FFVHs) in the upper plate of the WPF, with the most critical being FFVH 13. Such fatigue cracks jeopardise the structural integrity of the wing and could compromise the planned withdrawal date of 2020 of the aircraft. The RAAF manage the fleet by a safety-by-inspection approach based on the results of durability and damage tolerance analysis (DADTA). The purpose being to ensure growing cracks are detected before they reach critical length. Any process that can extend the inspection interval will potentially reduce RAAF F-111 maintenance costs significantly. Two possible mechanical approaches for life extension of these regions in the WPF are the AMRL designed stress-bridge, and non-circular cold expansion/interference-fit plug. The aim of these designs is to eliminate crack growth, or significantly reduce the rate.

Hence in the present investigation, F-111 representative static and fatigue testing has been undertaken to assess the suitability of AMRL designed stress-bridge and interference-fit plug options for the fatigue life enhancement of plates containing non-circular elongated holes of 2:1 aspect ratio. For the stress-bridge design, an improvement in strain concentration factor of 38% was demonstrated for lower magnitude remote loads as compared to plates with unenhanced holes. Conversely, during typical high loads, the alternating strain range was negligibly improved due to slipping of the feet. Hence during the fatigue tests there was extensive specimen cracking. However, excellent results were achieved with the interference-fit plug design, where the peak elastic strain concentration factor was reduced by 79% as compared to the unenhanced case. This design also prevented the introduction of detrimental residual tensile stresses during high loads. Consequently, for these enhanced specimens, crack growth during fatigue testing was completely prevented, and very large extensions in fatigue lives were demonstrated. Thus the interference-fit plug is considered a very suitable option for the fatigue life extension of elongated holes such as the critical fuel flow vent holes in the F-111 WPF.

Implementation of the interference-fit plug would be expected to provide significant cost savings and increased aircraft availability for the RAAF F-111 fleet. It would also be expected to extend the life of the F-111 aircraft by significantly reducing the risk of future instances of fatigue cracking at critical FFVHs. This would also be important in the context of achieving the aircraft planned withdrawal date.

Authors

R. L. Evans

Airframes and Engines Division

Rebecca Evans completed a Bachelor of Engineering in Aeronautical Engineering (with distinction) at the Royal Melbourne Institute of Technology in 1987. In 1988 she commenced work in Systems Division at DSTO Salisbury, where she worked on the design, analysis and testing of towed targets. Since 1992 she has been working in the Airframes and Engines Division where she has undertaken experimental and finite-element analyses of metallic aircraft components, evaluating various fatigue life-enhancement techniques.

M. Heller

Airframes and Engines Division

Manfred Heller completed a B. Eng. (Hons.) in Aeronautical Engineering at the University of New South Wales in 1981. He commenced employment in Structures Division at the Aeronautical Research Laboratory in 1982. He was awarded a Department of Defence Postgraduate Cadetship in 1986, completing a PhD at Melbourne University in 1989. He is currently a Principal Research Scientist and Functional Head for Structural Mechanics in the Airframes and Engines Division. His research contributions have focussed on the areas of stress analysis, structural shape optimisation, and bonded repair technology in the context of airframe life extension. Since 1992 he has led tasks which develop and evaluate techniques for extending the fatigue life of ADF aircraft components. He is a Corresponding Member on the Committee of Stress Analysis and Strength of Components, Engineering Science Data Units (ESDU) UK.

Contents

1. INTRODUCTION	1
1.1 F-111 Wing Pivot Fitting Cracking Background	1
1.2 Mechanical Life Extension Options	2
2. SPECIMEN CONFIGURATIONS.....	3
2.1 Strain Gauges	4
2.2 Unenhanced	4
2.2.1 Blueprint Specimens	4
2.2.2 Open-elongated-hole Specimens.....	5
2.3 Enhanced	5
2.3.1 Stress-bridge Specimens	5
2.3.2 Interference-fit Plug Specimens.....	6
3. EXPERIMENTAL METHODS	7
3.1 Static Calibration Testing.....	7
3.2 Determination of Representative F-111 CPLT Scaling Factor	8
3.3 Representative Specimen Fatigue Sequence	8
3.4 Specimen Fatigue Tests	9
4. RESULTS AND DISCUSSION.....	9
4.1 Elastic Calibration Strain Results	9
4.2 Typical CPLT Strain Results.....	10
4.2.1 Unenhanced Blueprint Specimens	10
4.2.2 Unenhanced Open-elongated-hole Specimens	10
4.2.3 Stress-bridge Specimens	10
4.2.4 Interference-fit Plug Specimens.....	11
4.2.5 Comparison of CPLT Results.....	11
4.3 Fatigue Lives and Crack Growth	12
4.3.1 Fatigue Lives	12
4.3.2 Crack Growth.....	12
5. CONCLUSIONS	13
6. ACKNOWLEDGEMENTS.....	14
7. REFERENCES.....	14
APPENDIX A: STRAIN-GAUGE RESULTS FROM SPECIMEN COLD PROOF LOAD TESTS	32
APPENDIX B: RAW STRAIN-GAUGE DATA FROM SPECIMEN COLD PROOF LOAD TESTS	45

1. Introduction

1.1 F-111 Wing Pivot Fitting Cracking Background

The wing pivot fitting (WPF) is a primary structural component in the F-111 wing and has been the site of fatigue cracking in service and structural failures during cold proof load testing (CPLT)¹. The WPF assembly, as shown in Figure 1, consists of an upper and lower plate with integrally forged stiffeners, which are welded together to form a box structure which transmits concentrated wing loads through a pivot pin. It is made of high strength D6ac steel that has low fracture toughness, hence it is sensitive to fatigue cracking in areas of high stress concentration. The main locations at which cracks have occurred are geometric features in the WPF upper plate stiffeners, known as fuel flow vent holes (FFVHs) and stiffener runouts (SROs). In terms of the FFVHs, the most frequent location of cracking has been at FFVH 13, however cracks have also been detected at FFVH 11, 12 and 14.

The unusual occurrence of fatigue cracking in the upper plate of the wing where the in-service flight loading is compression dominated is attributed to the presence of residual tensile stresses at the FFVHs and SROs, which is caused by localised material yielding during CPLT. These tensile residual stresses range in magnitude up to the material yield stress. Hence the normally compressive cyclic stresses due to in-flight manoeuvre load cycles are offset by the residual tensile stresses to become cyclic tensile stresses, making it susceptible to fatigue cracking. Such fatigue cracks in the FFVHs jeopardise the structural integrity of the wing and must be strictly managed in service. This imposes a huge (and costly) maintenance burden on the aircraft fleet in service with the Royal Australian Air Force (RAAF). The WPF is managed under a safety-by-inspection approach, based on the results of durability and damage tolerance analysis (DADTA). The purpose being to ensure growing cracks are detected before they reach critical length [1, 2]. In addition to the high costs involved, the aircraft availability is reduced and at current estimated crack growth rates the planned withdrawal date (PWD) of 2020 may not be achieved. The most critical FFVH is FFVH 13, and currently the RAAF have settled on a 1000 hourly (R4) inspection interval. Hence any measure, which justifies and allows extension of this interval can potentially produce large savings in RAAF F-111 maintenance costs, and provided it can be underpinned by a validated DADTA, will reduce the risk of in-flight failure.

Fatigue cracking in the upper plate is not a new problem and it is worth noting that significant prior measures have been undertaken as part of the fatigue management process. For example, 'short' cracks detected in the FFVHs have been removed by grinding, and then a specified surface finish is reinstated. Also, FFVH 13 is subject to a

¹ CPLT is a periodic proof load testing program performed in a special facility on the F-111 structure to confirm the absence of flaws above a small critical size. This then clears the aircraft for a further period of safe flight. In CPLT the aircraft is cooled to -40 °F (-40 °C) to embrittle the D6ac steel structure and then load cycles of -2.4 g and +7.33 g at 56° wing sweep angle, and -3.0 g and +7.33 g at 26° wing sweep angle are applied.

regular precautionary process called confidence polishing². However, these non-precise procedures have generally resulted in a large range of ill-defined FFVH shapes in the F-111 fleet. For the removal of 'long' cracks, AMRL developed a family of rework shapes for FFVH 13, [3]. Such a typical intermediate rework shape is shown in Figure 2. These shapes primarily addressed the stress concentration at the lower inboard corner of FFVH 13 by increasing the radius of curvature at that location, with the intention of reducing the peak residual tensile stress as well as the cyclic stress at this location. Fleet wings were reworked to a member shape of this family when a 'long' crack was detected in maintenance (small cracks were blended out by hand applied abrasion). A member shape was selected that was just large enough to completely remove the crack. The rework was manufactured using electro-discharge machining. It has been demonstrated by FE analysis and full-scale test that the family of standard FFVH 13 rework shapes gives a reasonable stress reduction at the critical lower inboard corner location. Unfortunately, the recent DADTA results, mentioned above, show that the stress reduction is not sufficient to produce an acceptable inspection interval. Also, there has been a recent instance of a crack at FFVH 13 in an F-111C wing, despite a rework shape similar to that shown in Figure 2 having been implemented previously in that wing³. These circumstances indicate that the current management strategy for FFVH 13, using the current rework shapes, is not sufficient to provide both an acceptable safe inspection interval and sufficient durability to the PWD.

1.2 Mechanical Life Extension Options

In view of the situation discussed above, improved or alternate cost-effective strategies are currently required to increase the inspection interval for F-111 wings. For an aircraft managed on safety-by-inspection, the most practical option for significantly improving the fatigue management of a critical location is to reduce the crack growth rate. For the existing structure, the key parameter that can be modified to reduce crack growth rate is the local stress conditions. For the critical FFVHs there are two important aspects, firstly the magnitude of the residual stress left after CPLT and secondly the magnitude of the cyclic stress due to in-service loading. In view of this problem, AMRL has in recent work developed two potential mechanical options for the life extension of the FFVH 13 region, with the aim of eliminating crack growth or significantly reducing the crack growth rate. The alternatives are firstly; a non-circular cold-expansion/interference-fit plug, and secondly a stress bridge [4] that is comprised of a reinforcement assembly clamped across the hole. The intent of both options is to reduce the stress concentration due to the open hole, and to inhibit the formation of residual tensile stresses (compression strains) which are present after the removal of the CPLT load. It should be noted that these mechanical options have been developed in parallel with another life extension

² Confidence polishing restores a R_a 8 μm surface condition and is applied to FFVH 13 only. The precise depth of material removed is unconfirmed, however it is estimated to be about 0.05–0.127 mm (0.002–0.005 in). It is applied after inspection, which generally occurs every 1000 hours for FFVH 13.

³ The first rework shape in wing A15-36 preceded the development of the Figure 2 shapes and appears to be based on a family of rework shapes recommended by Lockheed Martin Aeronautical Company (LMAC), the F-111 original equipment manufacturer. However, the radius at the lower inboard corner was similar to the radii in Figure 2, and hence it is anticipated to provide a similar stress reduction as the AMRL shapes.

alternative being developed in the Airframes and Engines Division. This being the specification and use of precise *optimal* rework shapes for FFVHs such as FFVH 13 which are designed by finite element analysis, [5].

For the interference-fit plug option there has been a significant degree of prior work. The concept is to accurately machine a non-circular hole to a size similar to the maximum AMRL rework shape as shown in Figure 2, for subsequent cold-expansion and interference-fitting. This would allow the repair to be applied to most holes in the fleet, irrespective of their current shape. The ability to cut such a hole with a high degree of accuracy has been demonstrated on an actual F-111 wing in prior work at AMRL, [6]. Here an advanced electro-discharge machining procedure was used. It is worth noting that interference fitting and/or cold expansion of circular holes are highly effective and well-known approaches [7, 8, 9], whereas the non-circular case is a relatively new concept. Two-dimensional finite-element analyses have recently been used to investigate the typical stresses for the non-circular hole enhancement [10, 11]. This work indicated that enhancement through combined cold expansion and interference fitting should be considerably better than interference fitting alone. Also in this work, plate stress distributions measured experimentally due to elastic interference-fitting to a level of approximately 0.74%, compared well with the finite-element predictions. This demonstrated the suitability of a proposed AMRL tapered plug/sleeve design to achieve effective elastic interference-fitting of an elongated hole. Cold-expansion testing of non-circular elongated holes using this proposed plug has also recently been undertaken [12]. Nominal expansion levels of greater than 2.5% were achieved along with maximum peak strains of more than 10,000 $\mu\epsilon$ and maximum residual strains of greater than 1600 $\mu\epsilon$, indicating highly effective cold expansion. It was also demonstrated that subsequent to cold expansion, interference fitting could be achieved without the need for post cold-expansion machining. Fatigue testing of the plug/sleeve assembly (with minor design revisions) was recommended to confirm its suitability as a highly effective option for extending the fatigue life of the FFVH 13 region of the F-111 aircraft.

Hence in this present investigation, representative static and fatigue testing of a D6ac steel plate with an elongated hole has been undertaken with the aim of determining the practical effectiveness and structural integrity of two mechanical life-enhancement options. Here a stress bridge (configuration #1 from [4]) and a slightly modified version of a cold-expansion/interference-fit tapered plug/sleeve design (i.e. changes in surface finish, and hole tolerances) which has been developed at AMRL [12], were tested. Initially in Section 2 the various unenhanced and enhanced specimen configurations are given. The experimental method used is then presented in Section 3. This is followed in Section 4 with the experimental results and discussion.

2. Specimen Configurations

For all tests the specimen plates were manufactured from D6ac steel, which was hardened to the same condition as the F-111 WPF. The plates are nominally 266 mm long, 76.2 mm wide with a thickness of 5 mm, as shown in Figure 3. All plates contain an elongated hole which is oriented at an angle of 16 degrees relative to the major (remote loading) axis. This locates the maximum hoop stress at the hole edge in the

same relative position as for the actual FFFVH 13 in the WPF [3]. Also the plate thickness represents the stiffener of the WPF and the precise cross-sectional geometry of each specimen is listed in Table 1. The specimens had no plasticity prior to testing. Four specimen enhancement cases were tested: (i) unenhanced blueprint hole, (ii) unenhanced open-elongated-hole (i.e. oversized), (iii) stress-bridge enhanced open-elongated-hole and (iv) interference-fit plug enhanced open-elongated-hole. The geometries of the hole varied with enhancement case, as discussed further in the following subsections.

2.1 Strain Gauges

Strain gauges were bonded to each of the plate specimens at locations shown in Figure 4. Gauges 1 and 3 were symmetrically positioned to read the maximum stress in the plate (i.e. at the expected critical location). The angular location of these two gauges was determined from prior finite-element analysis [13, 14]. Gauge 2 was located on the major axis of the hole and gauge 4 measured remote strain. Gauges 1, 2 and 3 were located *inside* the hole for the blueprint and stress-bridge specimens, as was the case for the wing test [15]. (Also, in this location the clamping pads of the stress-bridge assembly could not foul the gauges.) It was necessary to attach the strain gauges on the plate surface *adjacent* to the hole for the interference-fit plug specimens since the plug was assembled inside the hole. To enable a direct comparison between the unenhanced and the interference-fit plug specimens, the open-elongated-hole specimens and the plug specimens were strain-gauged alike (i.e. adjacent to the hole).

Micro-Measurements strain gauges and adhesive (M-bond 200) were used. Type EA-06-031MF-120 (used *inside* the hole only), EA-06-031DE-120, or EA-06-031DE-350 gauges were applied around the hole, and had a gauge length of 0.79 mm and a grid width of 0.81 mm. The remote gauge 4, was type EA-06-050AH-120, and had a gauge length of 1.27 mm and a grid width of 1.02 mm.

2.2 Unenhanced

2.2.1 Blueprint Specimens

The blueprint configuration had an elongated hole of the same geometry as was originally present in the FFFVH 13 location in the F-111 (refer to Figure 2). The geometry of the plate specimen is shown in the engineering drawing of Figure 5. The hole has an aspect ratio of 3:1, being 38.1 mm (1.50 in) long and 12.7 mm (0.50 in) wide. Apart from providing a comparison to the open-elongated-hole specimens, some of these specimens were used in preliminary static testing to determine the exact representative CPLT remote loading for all tests, as discussed further in Section 3.2. Four specimens were manufactured and tested. The test section as indicated in Figure 3 was 118 mm for the first two specimens, and then 95 mm for the last two specimens to ensure that buckling did not occur. This choice was based on prior work, which indicated that the test section of a typical FFFVH specimen should preferably be less than 110mm to maximise the buckling load [16].

2.2.2 Open-elongated-hole Specimens

The geometry of these specimens, Part number SE5/52/14/RS009-001, is shown in Figure 6. These specimens had a larger elongated hole than the blueprint case, and were used as a baseline for the enhanced specimens. The hole has an aspect ratio of 2:1, being 50.8 mm long and 25.4 mm wide. The size of this hole is similar to the maximum AMRL rework size (Figure 2), thus could be applied to most holes in the RAAF F-111 fleet irrespective of their current hole shape. To prevent buckling at the maximum compressive load, the test section was set at 95 mm. Thus, strain-gauge 4 (the remote gauge) was sacrificed under the test-machine grips. The reduced test section was of more importance than for the blueprint specimens as the minimum cross-sectional area was less for these open-elongated-hole specimens.

2.3 Enhanced

2.3.1 Stress-bridge Specimens

The first type of enhanced open-elongated-hole specimens were termed stress-bridge specimens and had a reinforcement assembly clamped across the hole providing an alternative load path [4]. The geometry and assembly of the bridge is shown in the engineering drawing of Figure 7, Part numbers SE 5/52/14/RS 173-001, -004 and -008 (configuration #1). The stress bridge is comprised of two retaining-plates, four clamping pads, eight roll pins and two 14 mm high-tensile bolts and nuts. Part of the remote load applied to the plate is transferred by friction through the retaining plates via the clamping pads, to effectively bypass the hole edge. Preliminary static testing was undertaken using different configurations of clamping pads, where it was concluded that configuration #1 without the outrigger bolt should be chosen for further studies [4]. This was due to its better linear performance and the fact that it provides higher pad pressures due to the lower pad areas. Prior to assembly all components of the bridge and the plate surface were cleaned with ethyl alcohol. The clamping pads were then attached to the retaining-plates via pinholes with the roll pins. The two halves of the bridge were fastened to either side of the open-elongated-hole specimen via the two high-tensile bolts and nuts, and these can be seen in Figure 8. A torque of 216 Nm was applied to the bolts. The test section ranged from 125 to 130 mm to ensure that the bridge did not foul the machine grips.

A total of four specimens were manufactured, assembled, and tested. The assembly of each specimen varied slightly, based on feedback from the designers during fatigue testing⁴. After the fatigue testing of specimen 1 the front surface of the retaining plates was marked due to fretting occurring between the plates and the clamping pads. The *back* surface of the retaining-plates from specimen 1 was used for specimen 2. The retaining-plates were remachined for the third specimen to remove all fretting material. In order to increase the friction between the pads and specimen plate it was decided to adhere the pads to the plate with araldite. However, the araldite failed under compressive load on a representative test article. It was then decided to locally roughen the clamping pads and specimen plate (with 120 grade carbide paper). The bolts were

⁴ Personal communication with A. Wong and D. Rowlands of AED, DSTO.

lubricated (with G-n Metal Assembly Paste) to increase the tension force per Newton-metre torque, and locknuts fitted.

It was believed that the arrangement of specimen 3 could be improved. Hence the friction/rolling difference was increased on both sides of the clamping pads for specimen 4. The pinholes were blocked on the specimen plate side. The retaining-plate/clamping pad surfaces were lubricated with the metal assembly paste (in the pinholes for the pads). The bolts were lubricated and locknuts fitted as for specimen 3 above.

2.3.2 Interference-fit Plug Specimens

The second type of enhanced open-elongated-hole specimens were termed interference-fit plug specimens. An interference fit plug/sleeve arrangement was used to achieve cold expansion and interference fitting of the elongated hole. The geometry and working details of the cold-expansion/interference-fit plug have been detailed in prior work [10, 12]. It is worth recapping the typical features of cold expansion and interference fitting. In the *cold expansion* process, a hole is expanded to a level sufficient to cause local yielding. This is achieved by passing an over-sized mandrel (in this case, a plug) through or partly through the hole. The plug is then removed and the surrounding elastically-deformed material forces a reduction in hole diameter from the fully expanded size. This results in a zone around the hole containing residual compressive hoop stresses. The mean of the induced local cyclic stresses due to an applied cyclic load is significantly less in the presence of the compressive zone at the hole boundary. *Interference fitting* is the process of installing an over-sized mandrel (plug) into a hole. Depending on the expansion level, either compressive or tensile (if there is no yielding) residual circumferential stress are induced in the plate at the hole boundary. The key benefit however is that the in-situ plug provides an alternative load path when the plate is subjected to remote cyclic loading, thus reducing the cyclic stresses in the plate at the hole boundary. It is noted that typically the greatest benefit to fatigue life extension, results from a combination of hole cold-expansion followed by interference fitting. In the present work the specimens experienced a one-stage cold-expansion/interference-fit process.

A schematic of the plug design is shown in Figure 9, and the engineering drawing is presented in Figure 10. The design is comprised of a stainless steel sleeve (bush), a high-strength tool steel (D2) tapered plug, a backing plate, spacers and two M12 bolts (which were high-tensile socket head screws). High-tensile nuts and washers were fitted to specimens 1 and 2 and locknuts to specimens 3 and 4. The mating surfaces of the plug and sleeve have a (nominal) 1:50 taper. As the plug is inserted (by tightening the bolts), the cross-sectional area of the plug increases and hence so does the amount of cold expansion. An important design feature is that there is no relative movement between the sleeve and the plate during plug insertion. A slit mid-way along one of the flat sides of the neat-fitting sleeve ensures that the cold-expansion process is not hindered. Figure 10 shows this slit (top middle of bush) and also shows that the flange on the opposite side is omitted. In the F-111 WPF, the FVH 13 is located adjacent to the upper plate (see Figure 1). Therefore, this design feature was required to prevent fouling of the sleeve flange and the upper plate in practical applications.

Prior to assembly all components of the plug assembly and the plate surface were cleaned with ethyl alcohol. The sleeve was inserted into the open-elongated-hole with the sleeve flange on the opposite side of the plate to the strain gauges. G-n Metal Assembly Paste was then used to lubricate the plug and the bolts. The plug was inserted from the sleeve flange side of the plate. To enable maximum insertion of the plug a 'plug removal tool' was used in place of the backing plate and spacers were used on top of the plug. Plug insertion distance (as defined in Figure 9), bolt torque and plate strain readings were taken as the plug was inserted.

Using the taper ratio of the outside of the plug (nominally 1:50, but actually 1:52.6), the level of interference can be determined from the plug insertion distance. Hence to achieve a nominal 1% radial interference, the plug needs to be inserted 6.68 mm into the hole. Insertion was deemed complete when strain gauge 2 was reading approximately 20,000 $\mu\epsilon$ or when the final insertion distance was between 0.5 to 1.0 mm (this corresponds to an insertion displacement of about 25 mm). These results can be seen graphically for specimens 2, 3 and 4 in Figures 11 to 16 (where plug insertion distance has been converted to actual displacement). The data for specimen 3 (Figures 12 and 15) show that the plug was inserted too far, and thus it was withdrawn slightly. Four specimens were manufactured, assembled, and tested with the interference-fit levels listed in Table 1. For the insertions, which reached a strain reading of approximately 20,000 $\mu\epsilon$, the nominal degree of interference (based on the initial radius at the end of the hole and the initial plug geometry), was between 3.4 and 3.9%. For specimen 1, only 5,200 $\mu\epsilon$ was reached resulting in a reduced interference fit of 2.4%, and hence this specimen was not correctly expanded (this specimen was used as a preliminary trial). A key point is that for all specimens, the assembly was then left in place to provide a combined cold-expansion and interference-fitting of the hole. The test section ranged from 102 to 105 mm. Photographs of an installed plug assembly can be seen in Figures 17 and 18.

3. Experimental Methods

Static and fatigue tests were conducted under load control using an Instron 500 kN test machine with PC interface to specify and monitor the load sequence applied. For the fatigue tests the average cyclic frequency used was 10 Hz (unless indicated otherwise). A total of 17 specimens were tested as follows; (i) four of the plate with unenhanced blueprint hole; (ii) three of the plate with unenhanced open-elongated-hole; (iii) four of the plate with stress-bridge enhanced open-elongated-hole, and (iv) four of the plate with interference-fit plug enhanced open-elongated-hole.

3.1 Static Calibration Testing

Prior to fatigue testing the specimens experienced an elastic static calibration of ± 100 MPa. The appropriate loads for each specimen were based on the precise cross-sectional geometries. To enable a direct comparison between all specimen types, the open-elongated-hole data have been factored to allow for the slight difference in strain-gauge location. Here using stress-bridge specimen 3, a static calibration was taken of the specimen plate only. The difference in strain readings due to the location of the strain gauges of the stress-bridge specimen plates (inside hole) and the open-elongated-hole

specimens and interference-fit plug specimen plates (adjacent to hole) could thus be determined. The results of this comparison can be seen in Figure 19. For clarity, only strain-gauge 3 data is presented in Figure 19b, as the gauge 1 and 3 data were virtually identical.

3.2 Determination of Representative F-111 CPLT Scaling Factor

From Reference [17] the F-111 aircraft CPLT cycle consists of a sequence of four loads, namely; -2.4 g, +7.33 g, -3.0 g and +7.33 g. The first two loads are at a wing sweep of 56° and the second two at 26° wing sweep. The CPLT is applied to the aircraft wings via a series of actuators. The resulting vertical shear and bending moment at the root of the wing due to this loading closely approximates the design limit.

Experimental data gathered from the strain survey of a full-scale test wing [15] indicated that the critical location of FFVH 13 sustained approximately -20,000 $\mu\epsilon$ for the maximum wing load case of +7.33 g. In the present work the corresponding location on the representative (blueprint) specimens experienced approximately -20,000 $\mu\epsilon$ at a peak compressive loading of -290 kN (see Section 4.2.1). Hence this is the nominal value of the peak compressive load used for all subsequent tests, unless noted otherwise. The tensile load to represent the -2.4 g wing loading was determined by using the results of prior FE of the open-elongated-hole specimen [13]. Here, for the critical region at the hole boundary in a plate specimen, it was found that remote loads of +138.3 kN: -252.4 kN are equivalent to the wing CPLT loading range of -2.4 g: +7.33 g. Hence scaling these FE results linearly, (to achieve a peak compressive load of -290 kN), gives loading magnitudes of +158.9 kN: -290 kN. These loads correspond to remote specimen tensile and compressive stresses of +418.98 MPa and -764.65 MPa respectively, (based on a gross area of 379.26 mm²). It should be noted that the difference in peak compressive load required achieving -20,000 $\mu\epsilon$ for the blueprint specimens, as compared to the prior FE work [13] is expected, as the blueprint specimens had a lower stress concentration factor than the open-elongated-hole specimens.

Four blueprint specimens were tested. The first three were used to determine the remote load required to attain strain of -20,000 $\mu\epsilon$ at the critical location of the hole. Hence only specimens 3 and 4 had the appropriate representative CPLT loading. More detail on the method and results of these tests is given in Sections 3.4 and 4.2.1 respectively.

3.3 Representative Specimen Fatigue Sequence

A flight-by-flight type load sequence dominated by compression was used. It was developed from the wing-pivot bending-moment history at the root of the wing of four instrumented F-111 aircraft [18]. Each repeated program was equivalent to 199 flights or 499.1 flying hours and consisted of 36,274 turning points, with a maximum compressive stress of $-0.403\sigma_{\max \text{ tensile}}$. The original load sequence had over 3.56×10^6 turning points, hence truncation was required to conclude the testing within a reasonable period of time. Each turning point was multiplied by -35 to convert the data from MIPS (million inch pounds) to MPa. A discriminant of 15% of the maximum value (83 MPa) was then applied to the spectrum, reducing it to 36,274 turning points. Thus, when the difference

between two consecutive turning points was less than 83, one was removed. The stress exceedance diagram of the spectrum for FFVH 13 is shown in Figure 20.

3.4 Specimen Fatigue Tests

Each F-111 aircraft undergoes CPL testing every 2000 hours (approximately). Hence to ensure that the specimens experienced a representative load history, CPLT loads were incorporated into the fatigue test. For all tests, unless otherwise noted, an initial CPLT was applied which consisted of the following stresses; 0, +418.98, 0, -764.65, 0, +418.98, 0, -764.65, 0 MPa, as determined above in Section 3.2. Subsequently, blocks consisting of a fatigue run of four programs (1996.4 flying hours) and a CPLT were then applied until the specimen failed, or the test was terminated and the specimen statically failed. The precise loads based on the slightly different cross-sectional areas for each specimen, which is equivalent to the above CPLT stresses, are listed in Table 1. The corresponding specimen loading to represent the maximum fatigue loading (-688.2 MPa) is also listed. This maximum fatigue loading was chosen to be equal to $0.9 \times$ maximum CPLT load. This factor was selected based on prior work [18] where representative static and fatigue spectrum loads were developed for the testing of an F-111 skin repair.

It should be noted that the CPLT applied to the specimens of -2.4 g, +7.33 g, -2.4 g, +7.33g, was not precisely correct, since the third load should have been -3.0 g. This error in the third load is considered to have a negligible effect on the results of the fatigue test, as the magnitude is small compared to the peak loads, and the strain response is in the linear range, as evidenced in Section 4, and it is only applied every 2000 simulated hours (approximately).

4. Results and Discussion

4.1 Elastic Calibration Strain Results

Table 2 summarises the average elastic strain concentration factor (K_t) results for gauges 1 and 3, for the four specimen types. Here the open-elongated-hole data have been factored to allow for the effect of strain-gauge location such that the results are for the 'inside hole' location, as discussed in Section 3.1. Separate results for strain gauges 1 and 3 have been listed for the asymmetrical stress-bridge specimens. It should be noted that for the stress-bridge specimens, only the tensile results were used as the compressive results were more non-linear, and data for both gauges are included due to the large variation between them. It can be seen that the extra load path that the stress bridge or interference-fit plug provide to the plate reduce the K_t significantly. However the interference-fit plug has the most substantial effect on K_t . Here the value of $K_t = 0.9$ has been achieved, as compared to $K_t = 3.8$ for the unenhanced blueprint hole and $K_t = 4.2$ for the open-elongated-hole. Hence there is no alternating stress concentration due to the presence of the filled hole.

4.2 Typical CPLT Strain Results

Strain data obtained during the CPL tests are presented in Appendices A (Figures A1 to A24) and B (Tables B1 to B24), respectively. Typical data are given for the first CPLT of each specimen.

4.2.1 Unenhanced Blueprint Specimens

As discussed in Section 3.2, the first three blueprint specimens were used to experimentally determine the representative CPLT loading. The strain data for the first CPLT (CPLT 1) for these four specimens are given in Figures A1 to A4 and the raw data are listed in Tables B1 to B4. (A data acquisition error in Table B3 for specimen 3 has been rectified for the data presented in Figure A3.) The figures show that the desired peak compression of $-20,000 \mu\epsilon$ was only fully reached for the testing of specimens 3 and 4. For the first specimen, the positive CPLT load, and the negative CPLT load (and hence fatigue loading) were 87% and 76% of the desired equivalent testing loads respectively, and 84% and 81% respectively, for the second specimen. The first three specimens were tested at a frequency of 5 Hz, while the fourth was tested at 10 Hz.

Hence when comparing with the other specimen configurations, only the strain results for specimens 3 and 4 should be used. For example for specimen 4, the key values were a peak compressive strain of $-20,244 \mu\epsilon$, peak tensile strain of $8,680 \mu\epsilon$ and residual strain of $-5,285 \mu\epsilon$.

4.2.2 Unenhanced Open-elongated-hole Specimens

The CPLT 1 strain data for each open-elongated-hole specimen are shown in Figures A5 to A7 and the numerical values are listed in Tables B5 to B7. The specimens had on average, peak compressive strains of $-23,000 \mu\epsilon$, peak tensile strains of $7,300 \mu\epsilon$ and residual strains of $-9,400 \mu\epsilon$.

4.2.3 Stress-bridge Specimens

For these specimens, strain response data for CPLT 1 and CPLT 31 are given in Figures A8 to A14, and the corresponding raw numerical data are given in Tables B8 to B14. It can be seen that the strain data for gauges 1 and 3 are dissimilar, and this is due to the asymmetric stress-bridge design. Even though the assembly of each specimen varied slightly, the CPLT 1 strain curves are very similar for specimens 1, 2 and 3, with peak compressive strains of approximately $-20,000 \mu\epsilon$ (gauge 1), and $-25,000 \mu\epsilon$ (gauge 3) and peak tension of approximately $7,000 \mu\epsilon$ (gauges 1 and 3). Hence for these specimens, the peak strain range is of the order of $27,000 \mu\epsilon$. The data also shows residual strains of approximately $-9,000 \mu\epsilon$ and $-12,000 \mu\epsilon$ for gauges 1 and 3 respectively. It can be seen that for specimen 3 the two hysteresis loops are quite distinct. It is worth noting the different strain results for specimen 4, since it failed unexpectedly at block 5. For this specimen the gauge 1 results are similar to the other specimens, however for gauge 3, there are more significant differences. For example the gauge 3 residual strains are $-5,204 \mu\epsilon$, as compared to about $-10,000 \mu\epsilon$ for the other three specimens. This indicates a different load transfer for specimen 4. The CPLT 31 data have also been included in

the appendices for completeness and future reference. However the reliability of the CPLT 31 data is uncertain due to the potential for fatigue-induced degradation of the gauges and the adhesive layer. Gauge 2 survived for all three relevant specimens and also gauge 4 for specimen 1.

All the above results for CPLT indicate that the stress bridge did not achieve the aim of minimising the peak compressive strains and the associated formation of detrimental residual compressive strains (i.e. tensile stresses).

4.2.4 Interference-fit Plug Specimens

Graphs of the strain data for CPLT 1 and CPLT 31 are given in Figures A15 to A21, and the corresponding numerical data are given in Tables B15 to B21. The strain responses for CPLT 1 data are similar for specimens 2, 3 and 4. This is expected since all these specimens had fully expanded holes. Here the residual tensile strains due to the interference fit (i.e. before CPLT 1) at gauge 2 are typically 20,000 $\mu\epsilon$. One important feature is that the peak strain range at the critical location has been reduced to about 15,000 $\mu\epsilon$ (see Figures A16, A18 and A20) during the CPLT 1, as compared to about 30,000 $\mu\epsilon$ for the open-hole specimens. This indicates the effectiveness of the design to significantly minimise the local alternating stresses, even for such high loads. Also, it can be seen that the local yielding in compression due to remote loading, as experience by the open-hole specimens, is completely avoided. Thus most importantly, the residual strain is positive, ranging from 460 to 1780 $\mu\epsilon$, indicating residual compressive hoop stresses. A peak interference strain of only 5,200 $\mu\epsilon$ was reached in specimen 1 as compared to an average of 20,000 $\mu\epsilon$ for specimens 2, 3 and 4. However, it can be seen that the alternating stress range for specimen 1, is similar to the other three specimens at gauge 2. The data for CPLT 69 data for specimens 2, 3 and 4 are included in Figures A22 to A24 and Tables B22 to B24 for completeness and future reference. Again, the reliability of these data is uncertain due to potential degradation in the adhesive and/or gauges.

The CPLT results for the fully expanded specimens indicate that the interference-fit plug achieved the aim of minimising the peak compressive strains and the associated formation of detrimental residual compressive strains.

4.2.5 Comparison of CPLT Results

To compare the effectiveness of the enhanced specimens during the CPLT loads, typical peak and residual strain gauge 1 results for CPLT 1 are presented together in Table 3 (excluding the preliminary results for blueprint specimens 1 and 2). The two sets of strain-gauge results for the stress bridge are (a) 'original' location (inside the hole) and (b) 'scaled' using the data of Figure 19 (adjacent to the hole). It can be seen that the scaled stress-bridge data shows only a small improvement on the unenhanced specimen data. This indicates that the beneficial effect of the stress bridge shown for the lower static calibration loading (see Section 3.1) is lost at the high CPLT loads. This is due to the loss of load transfer from slipped clamping pads. However, the results for the interference-fit plug are very good. There is a very significant reduction in the alternating strain range during all the CPLT loads and the residual strain is positive and hence beneficial.

4.3 Fatigue Lives and Crack Growth

Table 4 summarises the fatigue test results and includes crack length data at the nominal critical location as well as the maximum crack length. Here the fatigue lives are given in terms of blocks (see Section 3.4) along with the type of failure. Specimens which did not fail by fatigue were statically failed and the load required to do this is listed under the heading 'Residual strength'.

4.3.1 Fatigue Lives

For comparison with the other specimen configurations, only the results of specimen 3 and 4 for the blueprint configuration should be used. These two specimens had the appropriate loading magnitude applied as discussed in Section 4.2.1, throughout the fatigue testing. The average specimen fatigue life was 22 blocks. All the baseline open-elongated-hole specimens had identical fatigue lives of 2 blocks (i.e. 3,993 flying hours); hence fatigue testing of the fourth specimen was not undertaken.

Stress-bridge specimens 1 and 2 endured more than 31 blocks, which indicates a good life improvement over the baseline specimens. However, the structural integrity of this option was unsatisfactory, as discussed further in Section 4.3.2. Loud clicking was heard during the testing of the stress-bridge specimens. It is believed that this was due to slippage of the bridge assembly at high loads. The roll pins of the first two specimens sheared. Machining the retaining plate and clamping feet as one piece would overcome this problem. However, the serious amount of fretting (which was evident on the plate and pads of all specimens on disassembly) is not so easily amended.

The data presented in Table 4 clearly shows the excellent life extension improvement provided by the interference-fit plug. For the fully expanded specimens 2, 3 and 4, fatigue testing was terminated at 68.95 blocks (i.e. 137,652 flying hours) and the steel plate was statically failed after removal of the plug assembly. No cracks were detected in these specimens. The testing of specimen 1 was terminated at 32.71 blocks (i.e. 65,302 flying hours). Two small cracks were detected after static failure of this plate specimen, noting that the hole was not fully expanded. In all fatigue tests it was found that the interference-fit plug assembly moved to some extent within the elongated hole of the steel plate (even though the bolts remained tight). For specimen 3 the plug assembly was even slightly *inside* the sleeve flange (i.e. the insertion distance was negative (-0.25 mm) at block 59). Hence for any future practical implementation of this option, it is probably desirable to ensure locking of the plug with respect to the plate, after full plug insertion has been achieved. The plug assembly demonstrated very good structural integrity, surviving without damage (except for minor fretting) for more than 137,000 simulated flying hours.

4.3.2 Crack Growth

Fractographic work was performed on each of the four specimen types, [19]. Photographs of the typical fracture surfaces can be seen in Figure 21. The photographs (a, b and d) are of crack 1 which is located at the critical strain gauge 1 position (refer to Figure 4). The stress-bridge photograph (c) is of crack 2 (critical strain gauge 3 location).

Crack growth data for cracks 1 and 2 are presented graphically in Figure 22. Each crack was measured from its origin to the maximum point at the start of the CPLT (excluding the initial CPLT) i.e. in blocks, and is presented in Table 4. A more detailed analysis of the fractography of these FFVH 13 fatigue specimens has been undertaken, [19].

As can be seen from the photograph (Fig. 21a) and graph (Fig. 22) of the blueprint specimen type (specimen 3), the crack growth rate is initially high, with the crack initiating almost immediately, and then gradually reducing. This is expected to be due to two factors (i) the high residual tensile stress resulting from the CPLT, which are a maximum close to the hole boundary, and (ii) the fatigue loading which is dominated by compression. It is worth noting that the fractography data for the blueprint specimen type has been used in the validation of advanced fatigue crack growth modelling software. Figure 22 shows that the open-elongated-hole specimens have a very fast crack growth rate compared to the blueprint specimens. This is due to the higher value of $K_t = 4.2$ as compared to $K_t = 3.8$ for the blueprint specimens. Due to this higher K_t value, the magnitude and size of the detrimental residual tensile stresses (compressive strains) would be increased by the CPLT loading, as seen from the strain data (in Appendices A and B).

All of the stress-bridge specimens experienced significant cracking, as indicated in Table 4. In some cases cracking occurred at the anticipated open-hole critical location and in others it occurred elsewhere. For example, the largest cracks for specimens 1 and 3 were located adjacent to the clamping pads of the stress bridge. Figure 23 shows the extent of cracking of stress-bridge specimen 1, (the hole is distorted due to static failure of the plate and is cut to aid fractography). It can be seen that the clamping pads by design inhibited a large crack from growing in the crack 1 location, however crack 2 was 10.9 mm long. Also, the pads caused extremely large cracks to grow that were initiated by fretting. For example, crack 3 is 31.9 mm long.

All three interference-fit plug specimens that were fully expanded (i.e. to greater than 3%) had no detectable crack (at 500x magnification), which represents an excellent result. The interference-fit plug specimen 1, that was not fully expanded (i.e. 2.4%), had two extremely small cracks. Hence this fracture surface is only given in Figure 21, for completeness.

5. Conclusions

Representative static and fatigue testing has demonstrated that the AMRL interference-fit plug/sleeve design is highly suitable as a fatigue life extension option for elongated holes, such as the critical FFVHs in the F-111 WPF. This design significantly reduces the elastic strain concentration factor at the hole boundary to 0.9, as compared to 4.2 for the open-elongated hole case (i.e. oversize hole). It also prevented the introduction of residual tensile stresses during high CPLT loading, which would otherwise occur for open unenhanced holes. For all three specimens with fully expanded holes, crack growth during fatigue testing was completely prevented due to the introduction of beneficial residual compressive stresses and the reduction of the cyclic stresses. Also the interference-fit plug has proven structural integrity, enduring more than 137,000 simulated flying hours without any significant degradation. Implementation of the

proposed interference-fit plug to the F-111 fleet would be expected to provide significant cost savings by extending inspection intervals, and also increased aircraft availability for the RAAF.

The stress-bridge design is not recommended for the F-111 WPF context. It was found that for lower magnitude loads, the stress bridge reduced the peak elastic strain concentration factor in the plate to about 2.6 (as compared to 4.2 for the open-elongated-hole case). However, during the high CPLT loads the clamping pads slipped resulting in loss of load transfer. Hence the alternating strain range was not much improved as compared to the open-elongated-hole specimens, and significant residual tensile stresses were induced. There was significant specimen cracking at the critical location, as well as undesirable larger cracks near the bridge pads.

It is also noted that the present fatigue test results have been important for the validation of crack growth models used by AED for determining inspection intervals at critical F-111 structural locations.

6. Acknowledgements

The authors wish to thank Mr N.T. Goldsmith for his fractography work and Mr N.R. Absolom for his technical support. The authors also wish to acknowledge the helpful comments and suggestions provided by Mr K.C. Watters and Mr K.F. Walker.

7. References

1. **ANON.**, *RAAF F-111C Durability and Damage Tolerance Analysis Results*, Lockheed Martin Report FZS-12-5034, 15 September 1998.
2. **ANON.**, *RAAF F-111C Durability and Damage Tolerance Analysis Details*, Lockheed Martin Report FZS-12-5035, 15 September 1998.
3. **R.H. KEYS, L. MOLENT and A.D. GRAHAM**, *F-111 wing pivot fitting finite element analysis of rework of fuel flow vent hole #13*, Aircraft Structures Technical Memorandum 557, 1992, Aeronautical Research Laboratory.
4. **R.B. ALLAN and A. WONG**, *Experimental Stress Analysis of a Stress Bridge Life Extension Option for a Plate Containing an Elongated Hole Under F-111C Representative Loading Conditions*, DSTO File M1/9/297, Aeronautical and Maritime Research Laboratory.
5. **M. HELLER, M. BURCHILL, M. McDONALD and K.C. WATTERS**, *Shape optimisation of critical fuel flow vent holes in the F-111 wing pivot fitting*, DSTO-TR-1120, April 2001, Aeronautical and Maritime Research Laboratory.
6. **K. WALKER**, *Improved electrical discharge machining procedures for re-work of fuel flow vent hole No. 13 in F-111 wing pivot fitting*, Structures Laboratory Report No. 9/96, September 1996, Aeronautical and Maritime Research Laboratory.

7. **ANON.**, *Final report on phase II for D6ac bolt hole life improvement - F-111 coldwork modification development program*, General Dynamics Report, FZS-12-588, 10 April 1991.
8. **J.Y. MANN and G.S. JOST**, *Stress fields associated with interference fitted and cold-expanded holes, with particular reference to the fatigue life enhancement of aircraft structural joints*, Metals Forum, Vol. 6, No. 1, 1983.
9. **R.B. ALLAN and M. HELLER**, *Stress analysis of a plate containing a round hole with combined cold expansion and interference fitting under F-111C representative loading conditions*, DSTO-TR-0523, April 1997, Aeronautical and Maritime Research Laboratory.
10. **R.B. ALLAN and M. HELLER**, *Stress analysis of an interference fit life extension option for a cold expanded elongated fuel flow vent hole on the F-111C aircraft*, DSTO-TR-0549, June 1997, Aeronautical and Maritime Research Laboratory.
11. **M. HELLER, R.B. ALLAN and P. PIPERIAS**, *Stress analysis of an interference fit repair option for fuel flow vent hole 13 on the F-111C aircraft*, Proceedings of the First Australian Congress on Applied Mechanics, Melbourne, 21-23 February 1996, Vol. 1 pp. 151-158, 1996.
12. **M. HELLER, R.L. EVANS and R.B. ALLAN**, *Cold expansion tests for plates containing elongated holes*, DSTO-TN-0233, October 1999, Aeronautical and Maritime Research Laboratory.
13. **R.B. ALLAN**, *Elastic-Plastic Stress Analysis of a Plate with a Central Elongated Hole - Comparison of Experiment with Finite Element Analysis Containing the Unified Constitutive Material Model*, DSTO File M1/9/395, Aeronautical and Maritime Research Laboratory.
14. **J. PAUL, P. CHAPMAN and A. SEARL**, *Elastic/Plastic Finite Element Analysis of the F-111 Fuel Flow Vent Hole Number 13*, DSTO-TR-0454, November 1996, Aeronautical and Maritime Research Laboratory.
15. **K. LILLINGSTON**, *F-111 wing variable sweep strain survey*, AED, Structures Laboratory Report no. 8/95, November 1995, Aeronautical and Maritime Research Laboratory.
16. **R.B. ALLAN**, *Experimental Stress Analysis of a Plate Containing an Elongated Hole to Determine Buckling Behaviour Under Representative F-111C Loading Conditions*, DSTO-TN-0073, March 1997, Aeronautical and Maritime Research Laboratory.
17. **ANON.**, *Test Loads and General Test Procedures for F-111 Proof Testing Phase III Structural Inspection Program F-111 A/E/D/F/FB-111A*, General Dynamics Fort Worth Report FZS-12-360A, November 1985.
18. **K. WALKER and G. SWANTON**, *Static and Fatigue Test Loading Development for an F-111 Bonded Composite Repair Substantiation*, DSTO-TN-0063, November 1996, Aeronautical and Maritime Research Laboratory.
19. **N.T. GOLDSMITH**, *Fractography of D6ac Steel Specimens Representing Fuel Flow Vent Hole 13 in F-111 Aircraft*, DSTO Report, Aeronautical and Maritime Research Laboratory.

Table 1. Specimen geometry and loading.

Enhancement case ^a	Width (mm)	Thickness (mm)	Area (mm ²)	Load (kN) equivalent to CPLT +418.98 MPa	Load (kN) equivalent to CPLT -764.65 MPa	Load (kN) equivalent to fatigue -688.2 MPa
Blueprint hole						
1 ^b	76.06	4.99	379.54	159.02	290.22	261.20
2 ^c	76.21	4.97	378.76	158.69	289.62	260.66
3	76.31	4.97	379.26	158.90	-290.00	-261.00
4	76.27	5.334	406.82	170.45	-311.08	-279.97
Open-elongated-hole						
1	76.31	5.07	386.89	162.10	-295.84	-266.25
2	76.18	5.10	388.52	162.78	-297.08	-267.37
3	76.24	5.33	406.36	170.26	-310.72	-279.65
Stress bridge						
1	76.18	5.12	390.04	163.42	-298.24	-268.42
2	76.305	5.095	388.77	162.89	-297.27	-267.55
3	76.24	5.13	391.11	163.87	-299.06	-269.16
4	76.27	5.33	406.52	170.32	-310.84	-279.76
Interference-fit plug^d						
1 (2.4%)	76.15	5.13	390.65	163.67	-298.71	-268.84
2 (3.4%)	76.08	5.125	389.91	163.36	-298.14	-268.33
3 (3.9%)	76.21	5.35	407.72	170.83	-311.76	-280.59
4 (3.7%)	76.39	5.125	391.50	164.03	-299.36	-269.42

a Blueprint specimens 1, 2 and 3 were tested at 5 Hz; all other specimens were at 10 Hz.

b In this preliminary CPLT and fatigue testing, the actual applied positive and negative CPLT loads were 87% and 76% of the tabulated values. The fatigue sequence loads were 76%.

c In this preliminary CPLT and fatigue testing, the actual applied positive and negative CPLT loads were 84% and 81% of the tabulated values. The fatigue sequence loads were 81%.

d Level of nominal interference fit in brackets. This first specimen was not fully expanded; hence strain and fatigue results are not representative of the proposed option.

Table 2. Comparison of averaged strain results for specimens during ± 100 MPa static calibration loading at the critical location (inside the hole).

Enhancement case	Approx. normalized strain range ($\mu\epsilon$)	Approx. strain concentration ^a
Blueprint open hole	3700	3.8
Open-elongated-hole ^b	4100	4.2
Stress bridge in elongated hole ^c	1900, 2600	1.9, 2.6
Inter.-fit plug in elongated hole	960	0.9

a Remote strain value was calculated using the applied load and Hooke's Law.

b Data has been scaled to allow for difference in strain gauge locations (i.e. inside hole compared to adjacent surface).

c Only strain results for tensile loading were used. Data for gauges 1 and 3 are included due to the asymmetry of the specimens.

Table 3. Typical strain gauge 1 results during CPLT 1 (including stress bridge data scaled for strain gauge location differences).

Load case	Strain ($\mu\epsilon$)				
	Blueprint hole	Open-elongated hole	Stress bridge in elongated hole		Inter.-fit plug in elongated hole
			original	scaled	
Peak tension	8680	7429	6084	4715	8011
Peak compression	-20244	-21707	-21624	-16759	-3857
Residual	-5285	-9375	-10584	-8203	1260

Table 4. Specimen fatigue test results.

Enhancement case	Fatigue life (blocks)	Failure type	Crack length (mm) Crack 1, Crack 2 (from Ref. [19])	Maximum crack length (mm) (from Ref. [19])	Residual strength (kN)
Blueprint hole					
1	31 ^a	Test terminated	2.7, 2.3	2.7	288
2	31 ^a	Test terminated	3.6, 2.6	3.6	275
3	23	Fatigue	16.3, 15.9	16.3	n/a
4	21	Fatigue	16.6, 17.2	17.2	n/a
Open-elongated-hole					
1	2	Fatigue	10.6, 12.6	12.6	n/a
2	2	Fatigue	21.9, 24.6	24.6	n/a
3	2	Fatigue	19.3, 17.5	17.5	n/a
Stress bridge in elongated hole					
1	31 ^b	Test terminated	- , 10.9 ^c	31.9 ^c	196
2	31	Test terminated	4.9, 10.8	10.8	159
3	31	Fatigue	- , -	42.0 ^c	n/a
4	5	Fatigue	4.8, 18.3	18.3	n/a
Interference-fit plug in elongated hole					
1 ^d (2.4%)	33	Test terminated	0.5, 0.2	0.5	344
2 (3.4%)	69	Test terminated	0.0, 0.0	0.0	341
3 (3.9%)	69	Test terminated	0.0, 0.0	0.0	367
4 ^e (3.7%)	69	Test terminated	0.0, 0.0	0.0	345

a Fatigue life was actually 30 blocks and 1.7 programs. Approximately 81% of the value of the full loading magnitude was applied.

b Fatigue life was actually 30 blocks and 1.78 programs.

c Crack initiated under the clamping pads of the stress bridge.

d This specimen was not fully expanded hence fatigue and crack results are unrepresentative of the enhancement case. Fatigue life was actually 32 blocks and 2.84 programs.

e Four loads of between 122 kN and 175 kN were inadvertently applied before the 2nd CPLT.

- Crack was not measured.

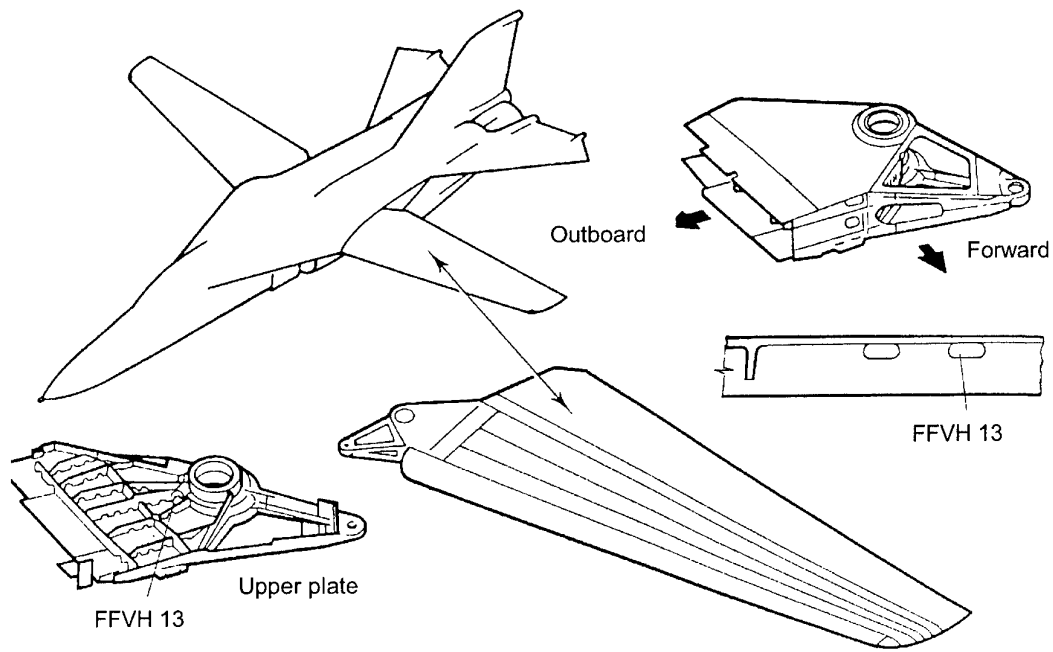


Figure 1. F-111 aircraft and wing showing the location of fuel flow vent hole number 13 (FFVH 13) in the wing pivot fitting (WPF).

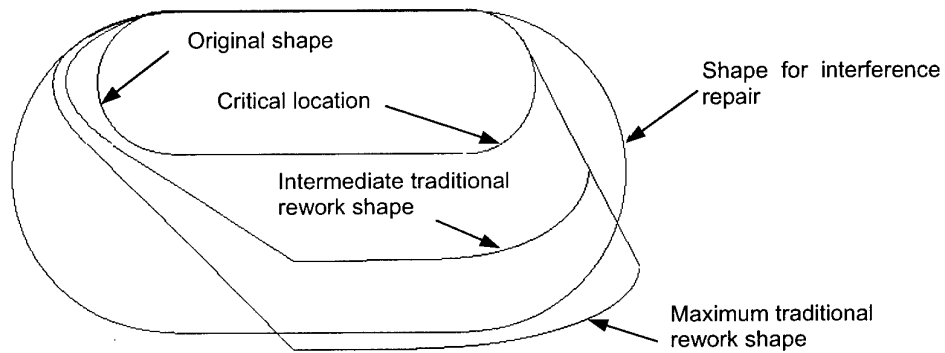
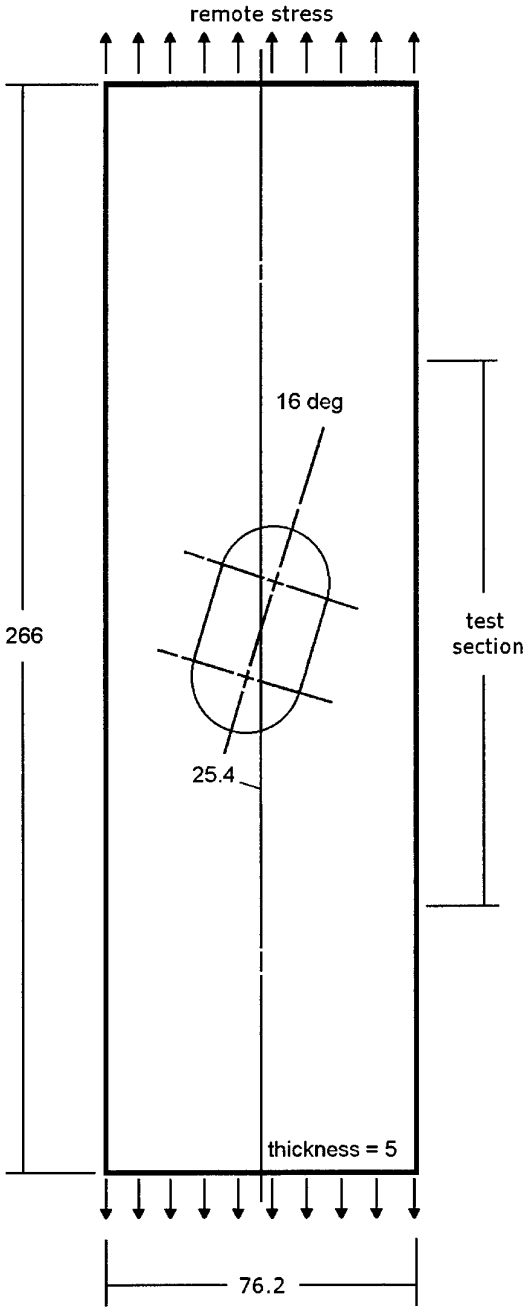
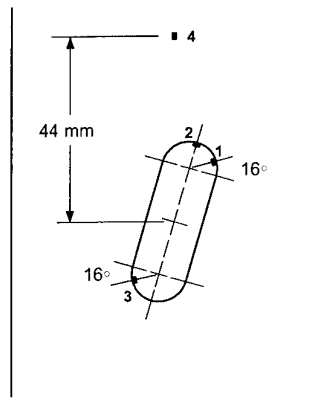


Figure 2. Comparison of the original (i.e. blueprint) geometry of FFVH 13 with typical RAAF rework shapes and proposed hole for interference-fit plug.

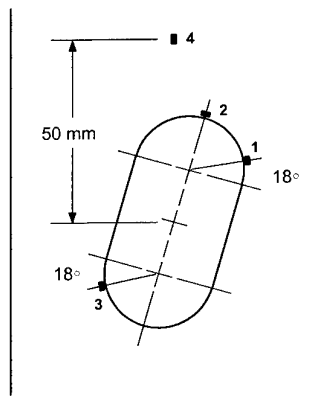


All dimensions in mm

Figure 3. Nominal geometry of specimen plates with hole.

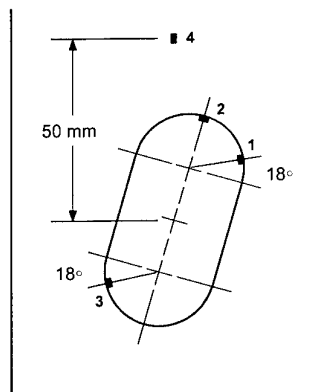


(a) *Blueprint*



The centres of strain gauges 1, 2 and 3 are a maximum distance of 0.5 mm from the hole edge.

(b) *Open-elongated-hole and interference-fit plug*



(c) *Stress bridge*

Figure 4. Strain-gauge locations for specimens.

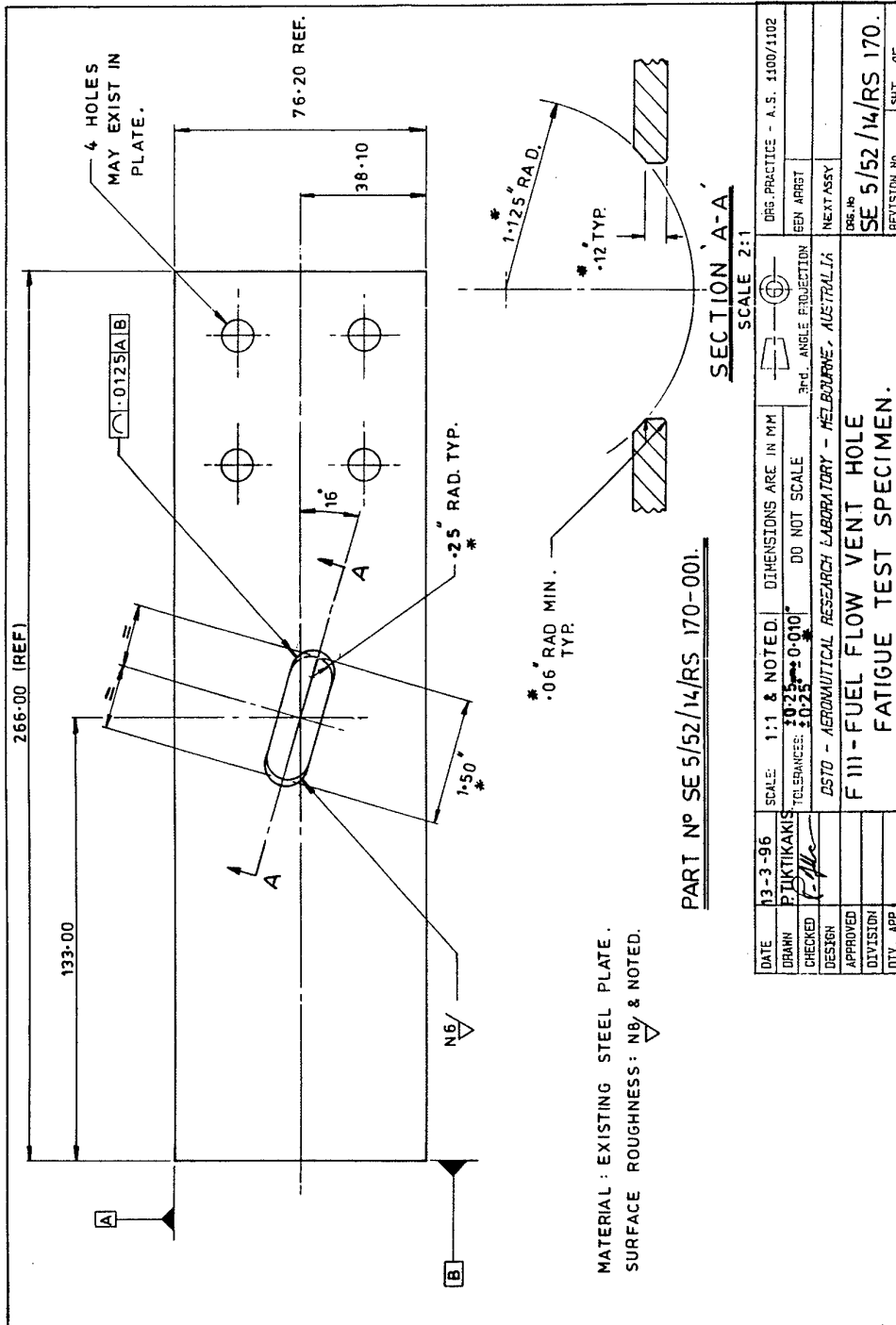
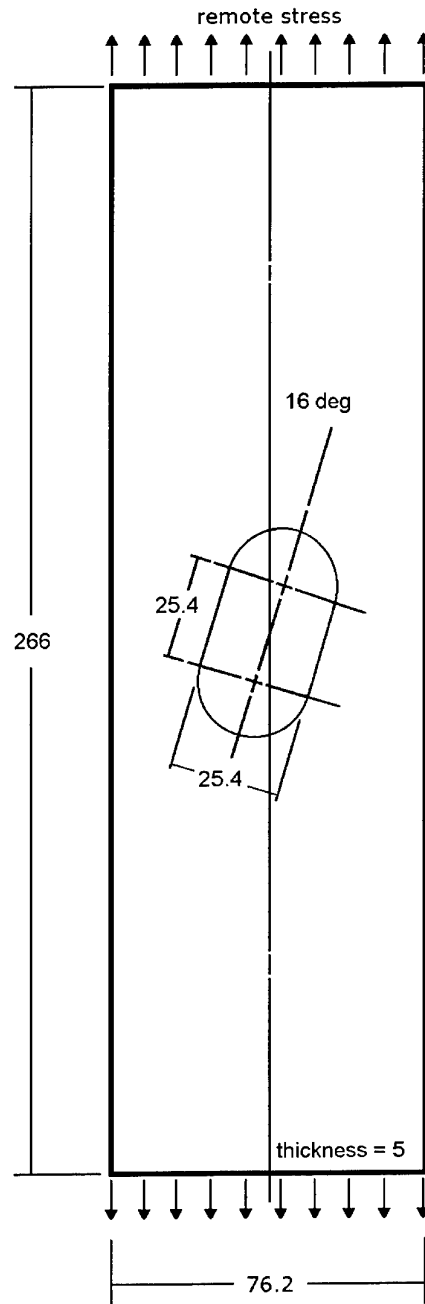


Figure 5. Engineering drawing of blueprint specimen plates.



All dimensions in mm

Figure 6. Nominal geometry of open-elongated-hole specimens, stress-bridge and interference-fit plug plates.

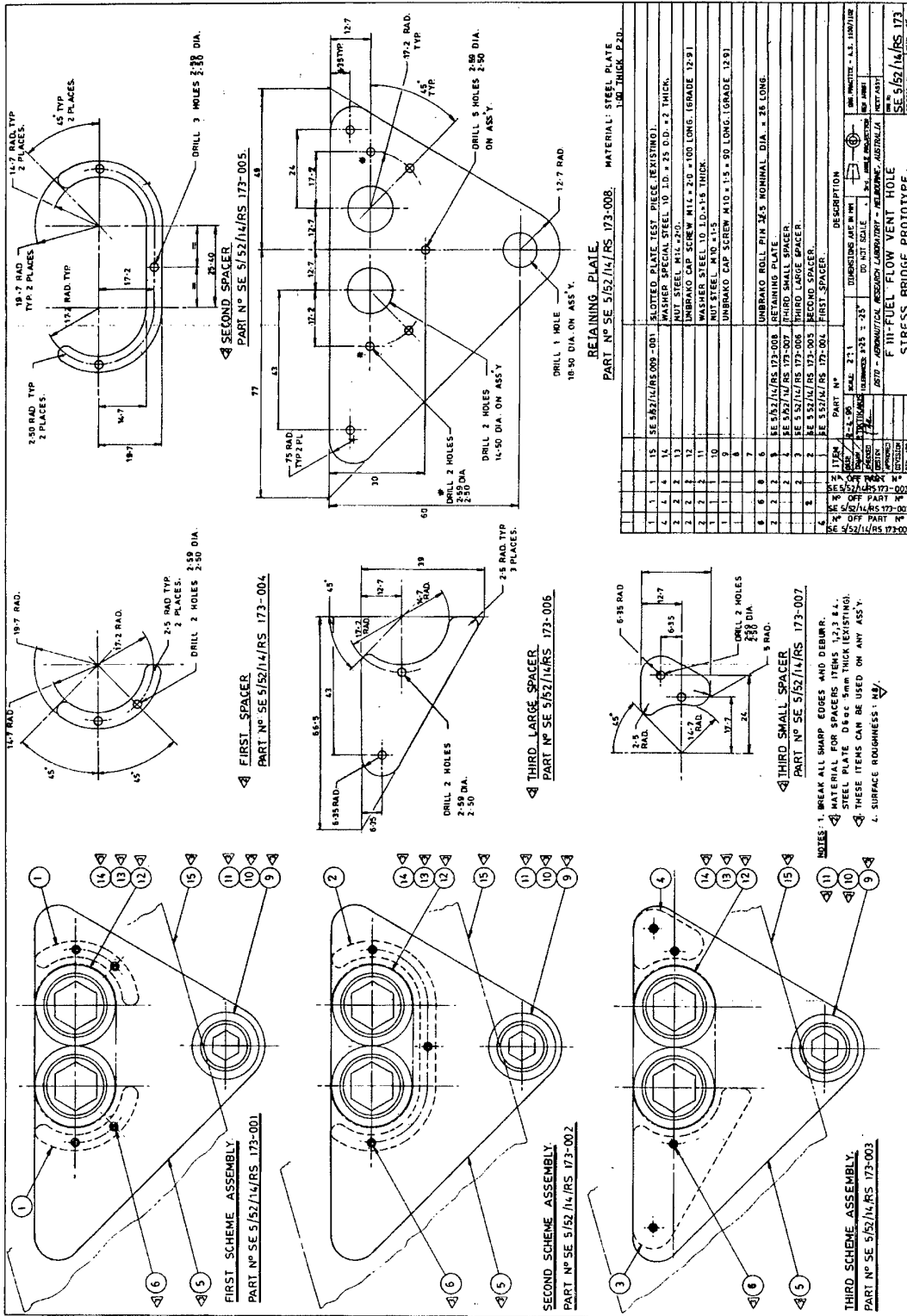


Figure 7. Engineering drawing of stress-bridge assemblies (present work used First Scheme Assembly, excluding items 9,10 & 11).



Figure 8. Assembled stress-bridge specimen 1 in the fatigue test machine.

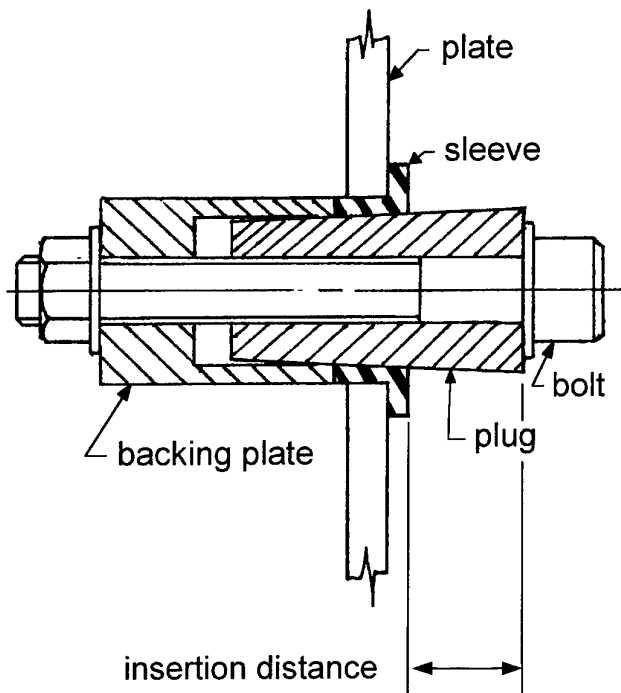


Figure 9. Schematic of the interference-fit plug/sleeve design inserted in to a plate with an elongated hole.

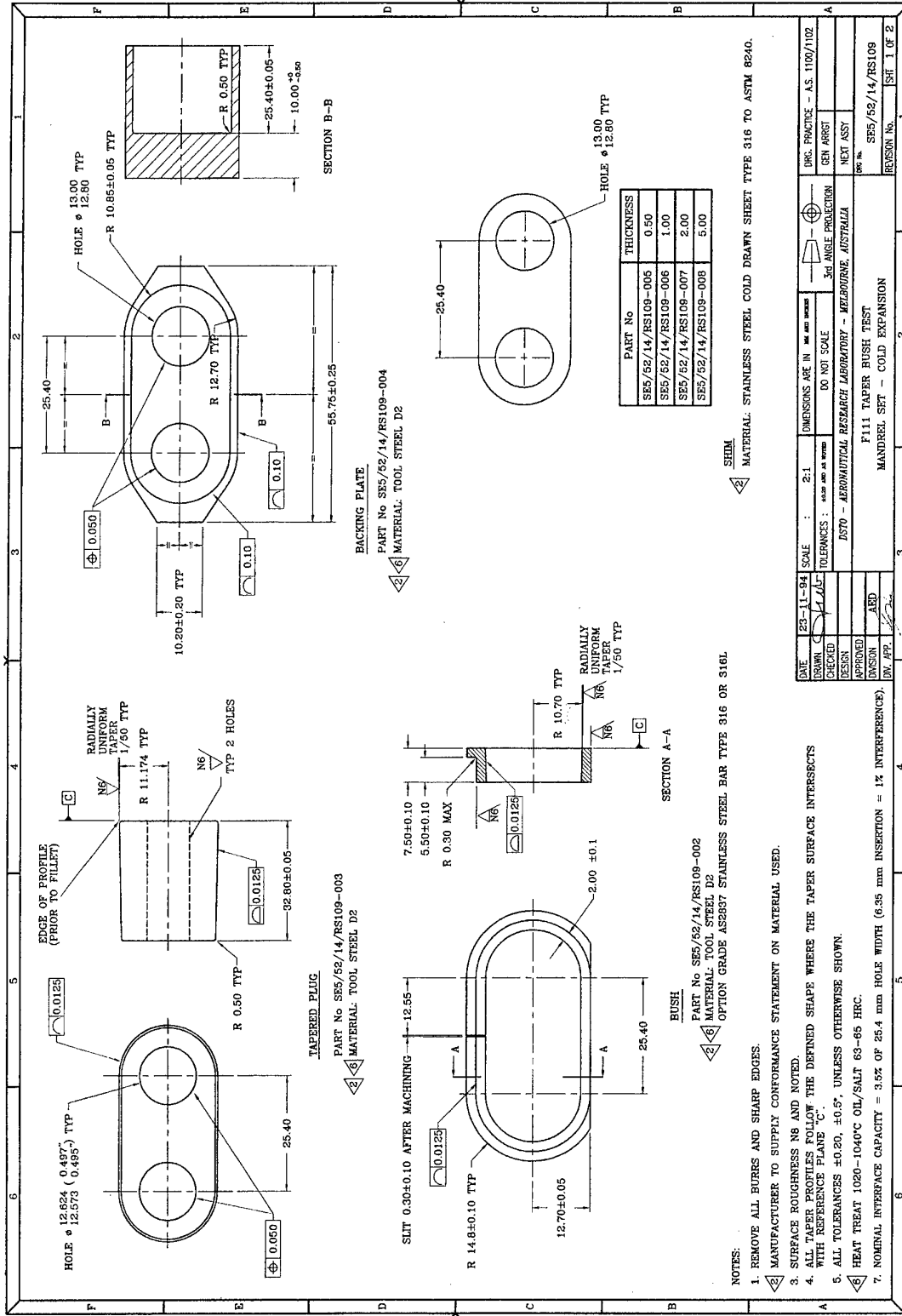


Figure 10. Engineering drawing of components for the cold expansion/interference-fit plug.

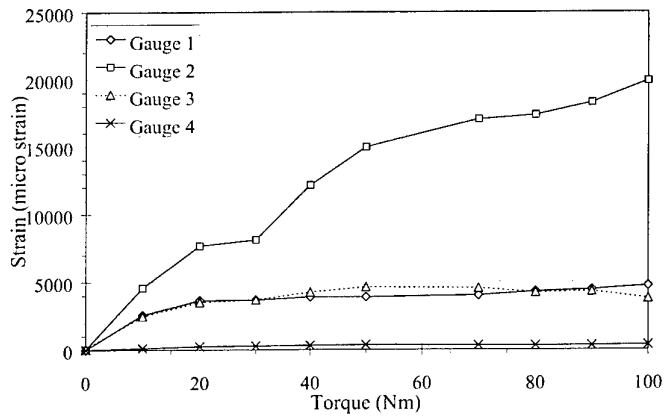


Figure 11. Strain vs Torque for interference-fit plug specimen 2.

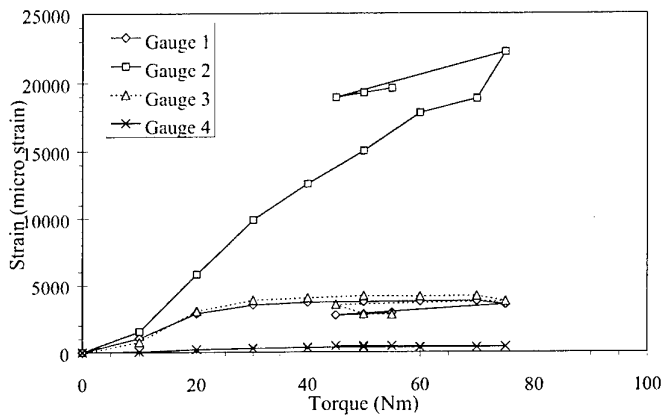


Figure 12. Strain vs Torque for interference-fit plug specimen 3.

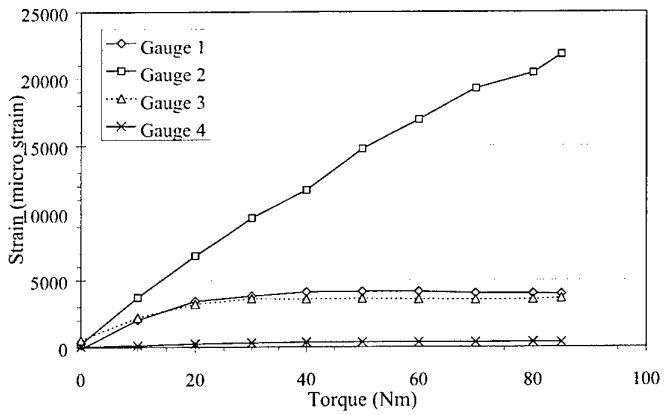


Figure 13. Strain vs Torque for interference-fit plug specimen 4.

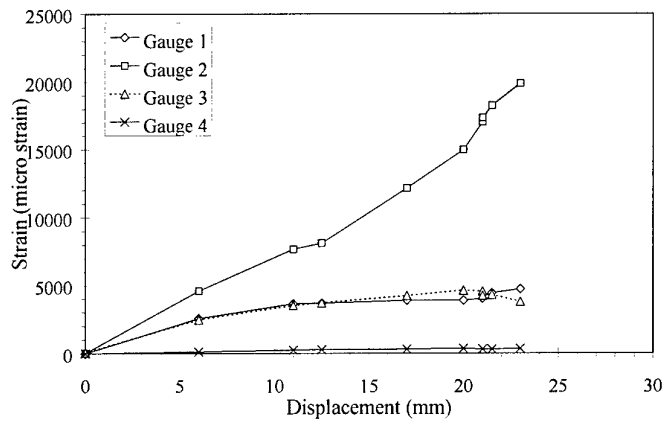


Figure 14. Strain vs Displacement for interference-fit plug specimen 2.

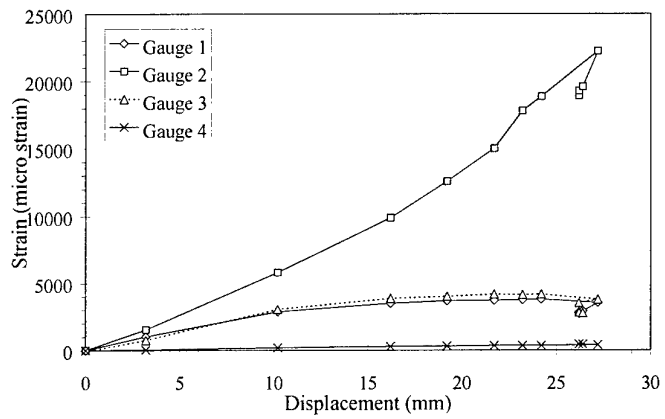


Figure 15. Strain vs Displacement for interference-fit plug specimen 3.

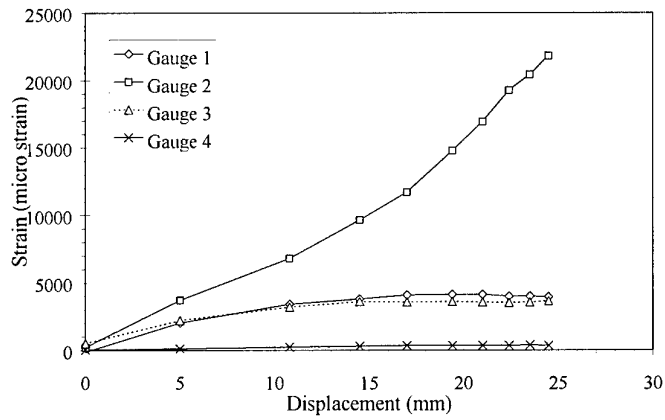


Figure 16. Strain vs Displacement for interference-fit plug specimen 4.

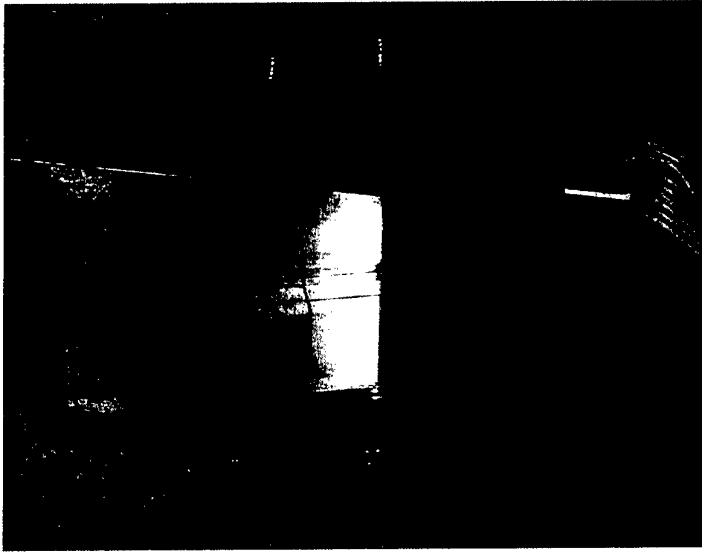


Figure 17. Plug assembly installed in interference-fit plug specimen 1.

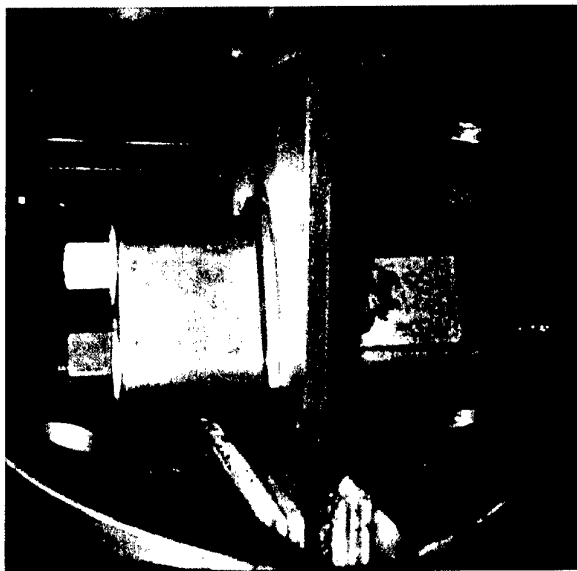
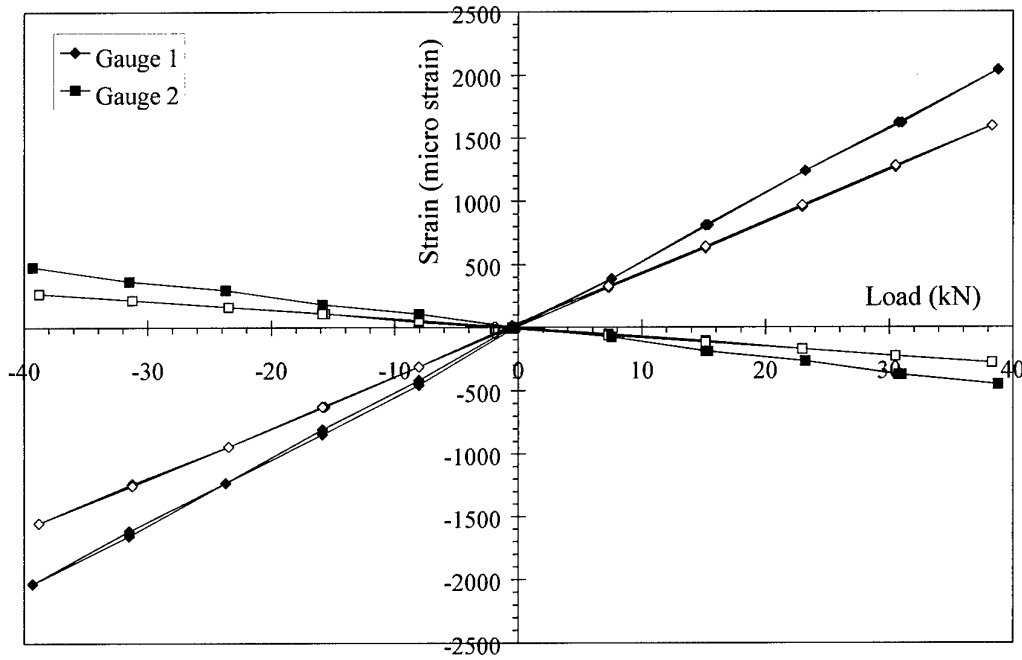
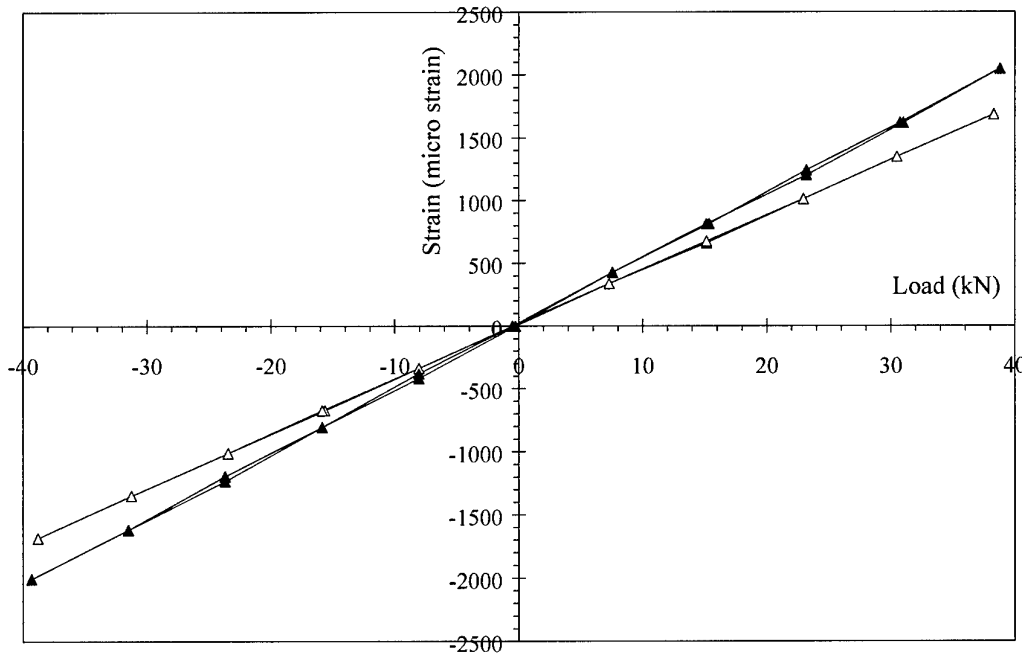


Figure 18. Interference-fit plug specimen 2 during fatigue testing.



(a) Strain gauges 1 and 2



(b) Strain gauge 3

Figure 19. Effect of strain-gauge location on strain data, with open symbol for adjacent to hole (open-elongated-hole specimen 1), and solid symbol for inside hole (plate only of stress-bridge specimen 3).

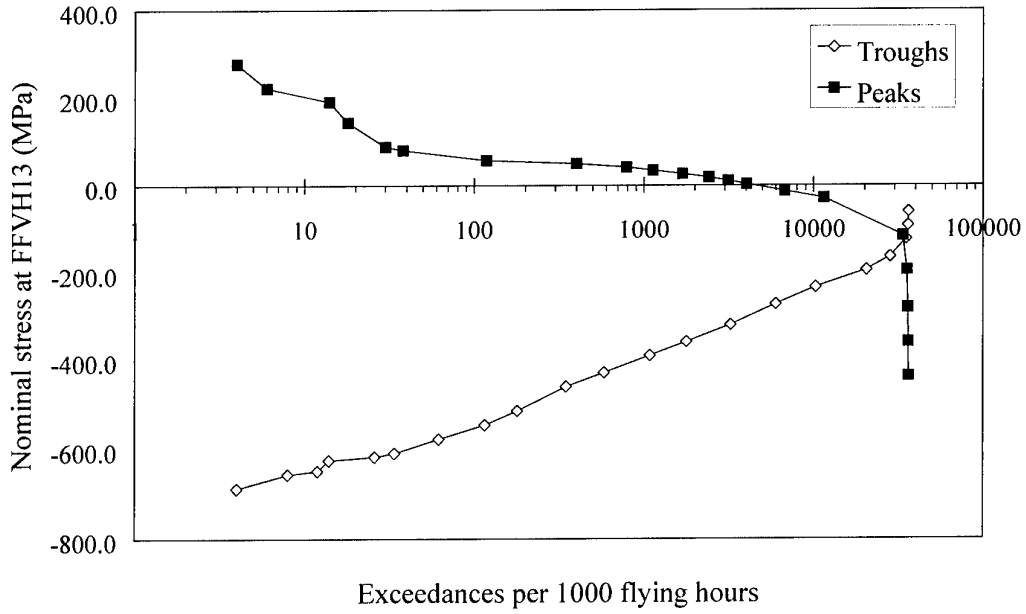
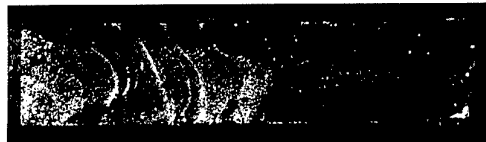


Figure 20. Stress exceedance diagram.



(a) Blueprint



(b) Open-elongated-hole



(c) Stress bridge



(d) Preliminary interference-fit plug
(crack of 0.5 mm at lower LH corner,
noting hole not fully expanded)

Figure 21. Photograph of typical fracture surfaces of each of the four specimen types (where specimen thickness is 5 mm).

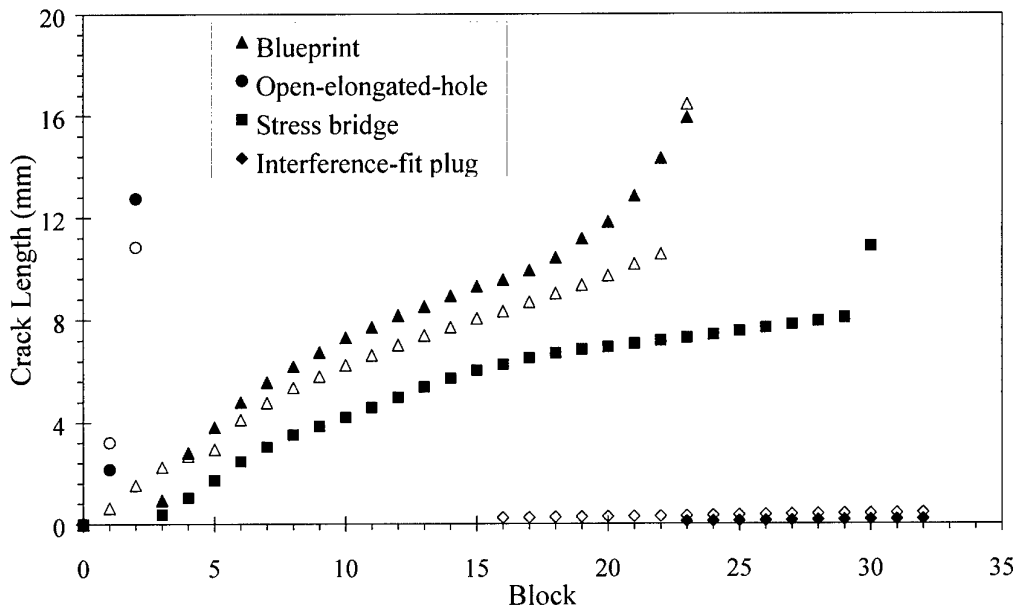


Figure 22. Sample crack growth results, with open symbol for crack 1 and solid symbol for crack 2, (noting that interference plug results are for preliminary case where hole was not fully expanded).



Figure 23. The plate of stress-bridge specimen 1 after static failure.

Appendix A: Strain-gauge results from specimen cold proof load tests

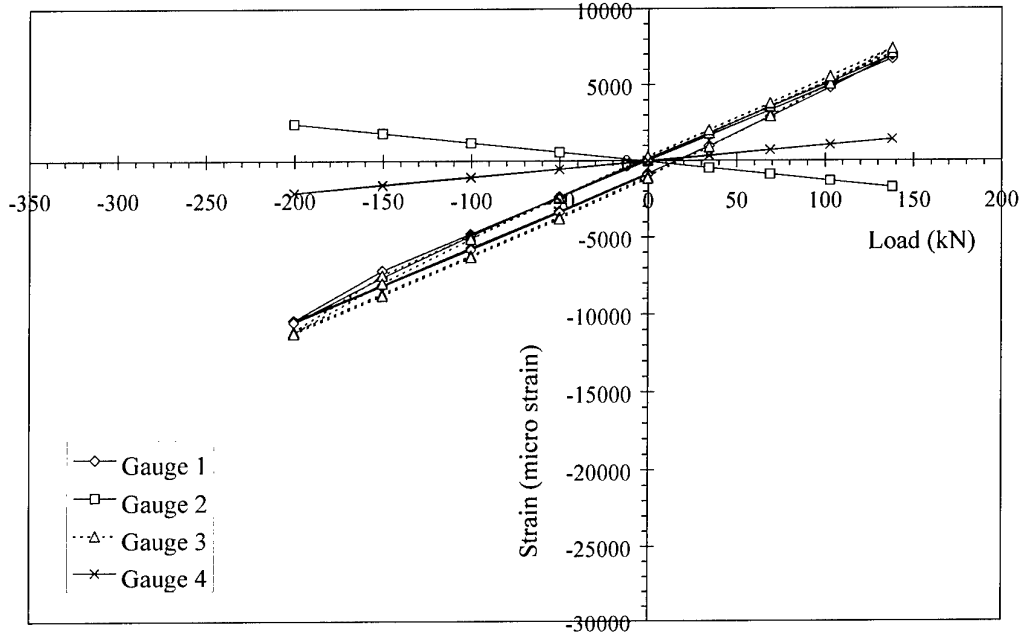


Figure A1. CPLT 1 for blueprint specimen 1.

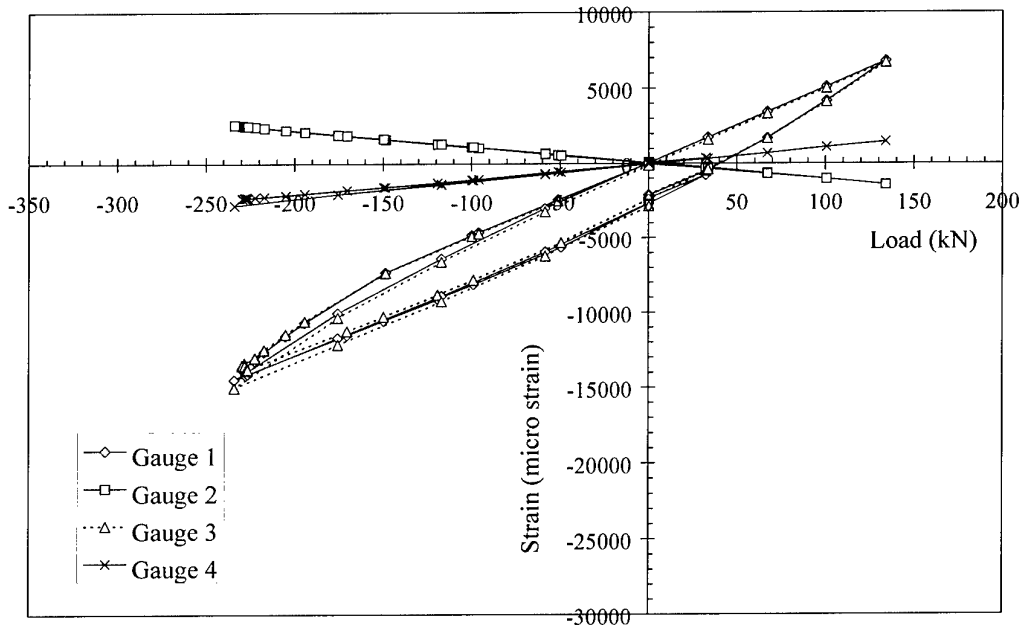


Figure A2. CPLT 1 for blueprint specimen 2.

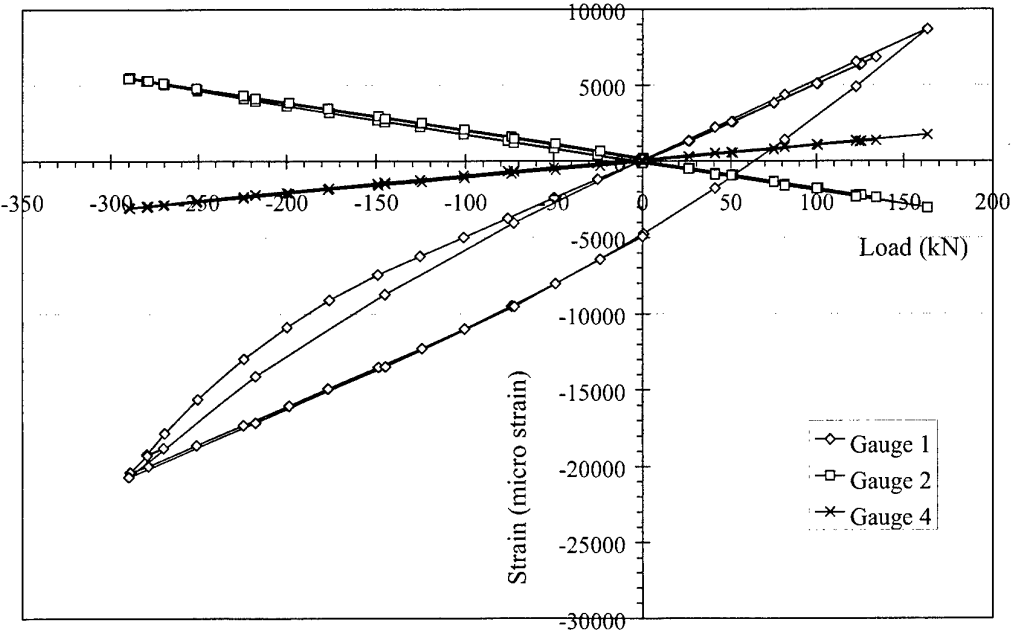


Figure A3. CPLT 1 for blueprint specimen 3.

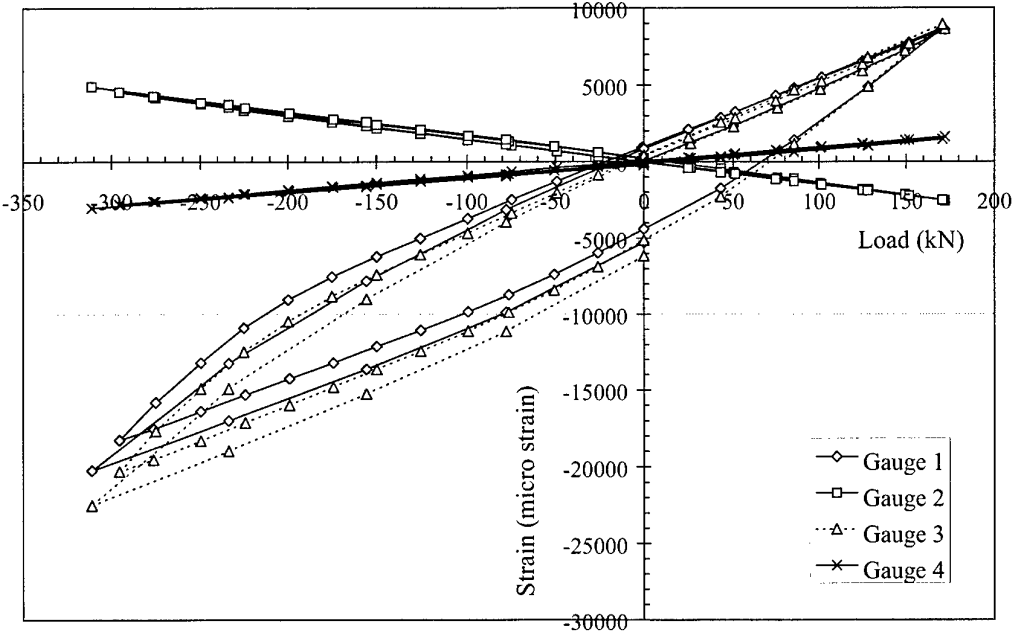


Figure A4. CPLT 1 for blueprint specimen 4.

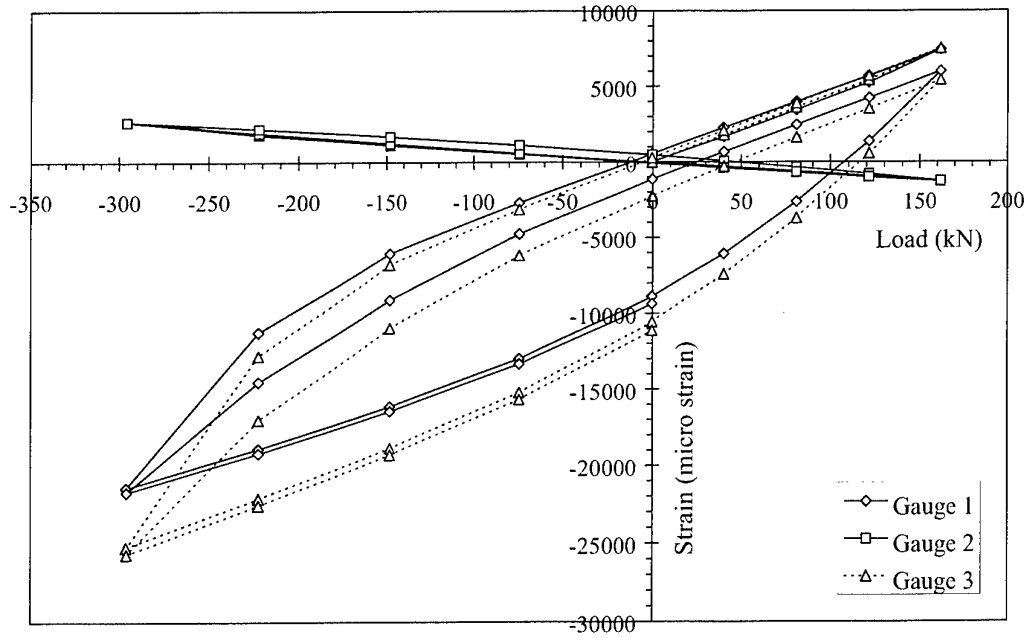


Figure A5. CPLT 1 for open-elongated-hole specimen 1.

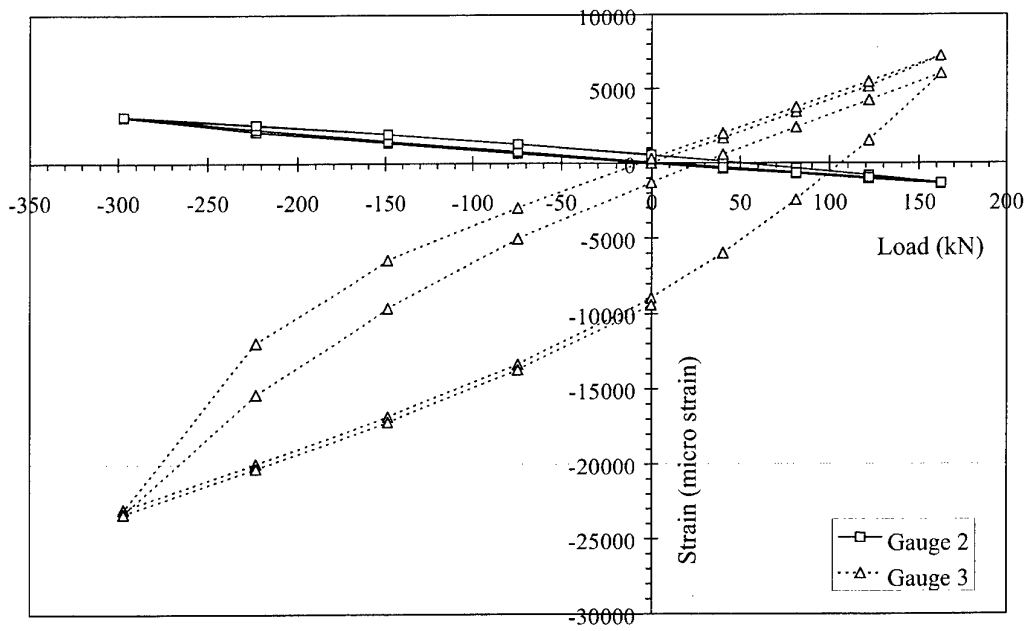


Figure A6. CPLT 1 for open-elongated-hole specimen 2.

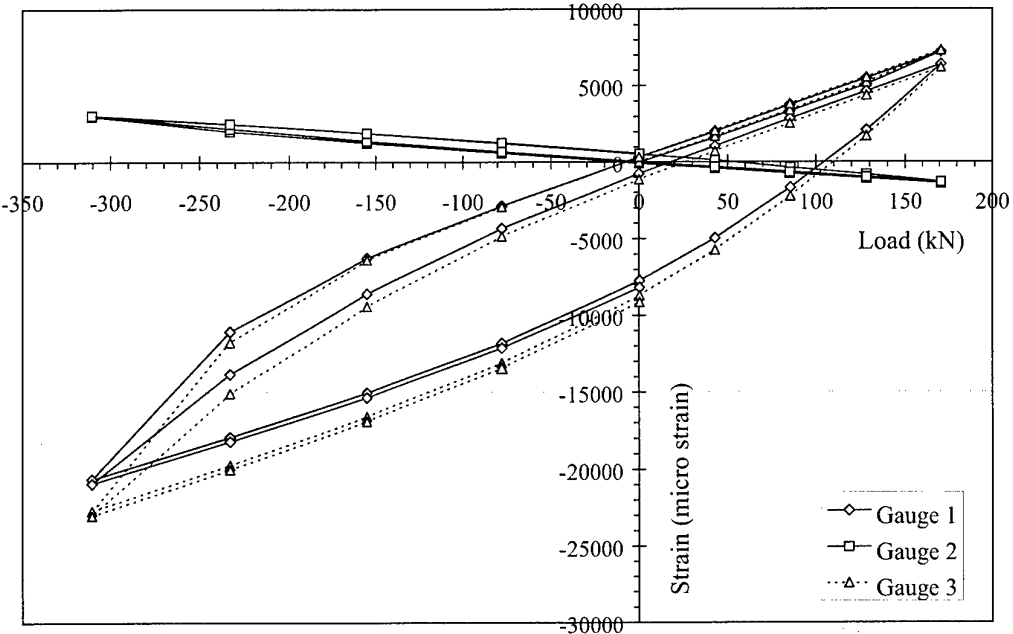


Figure A7. CPLT 1 for open-elongated-hole specimen 3.

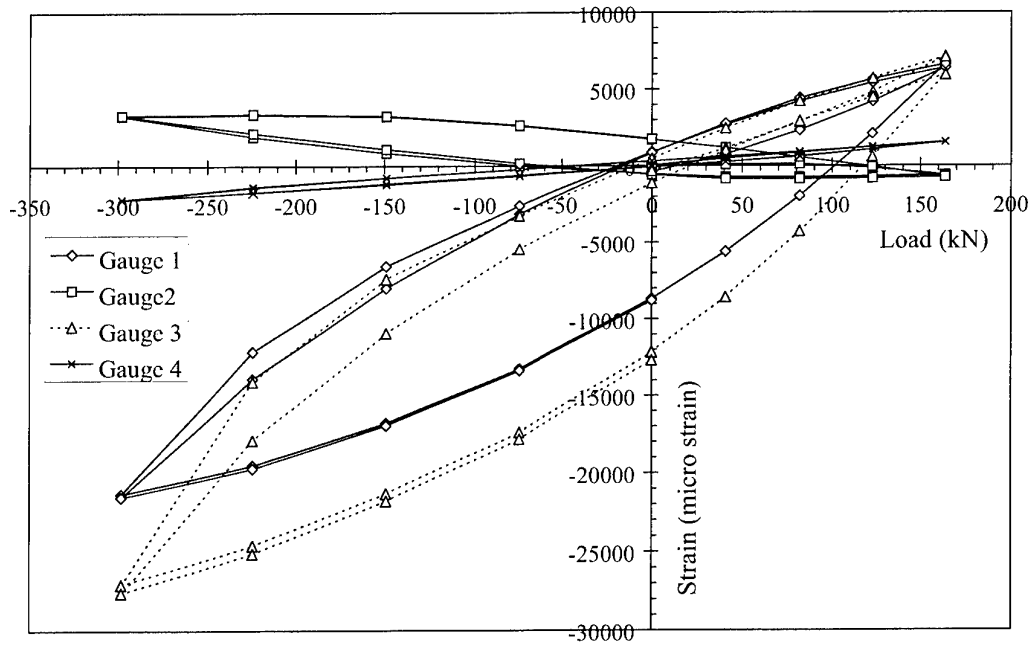


Figure A8. CPT 1 for stress-bridge specimen 1.

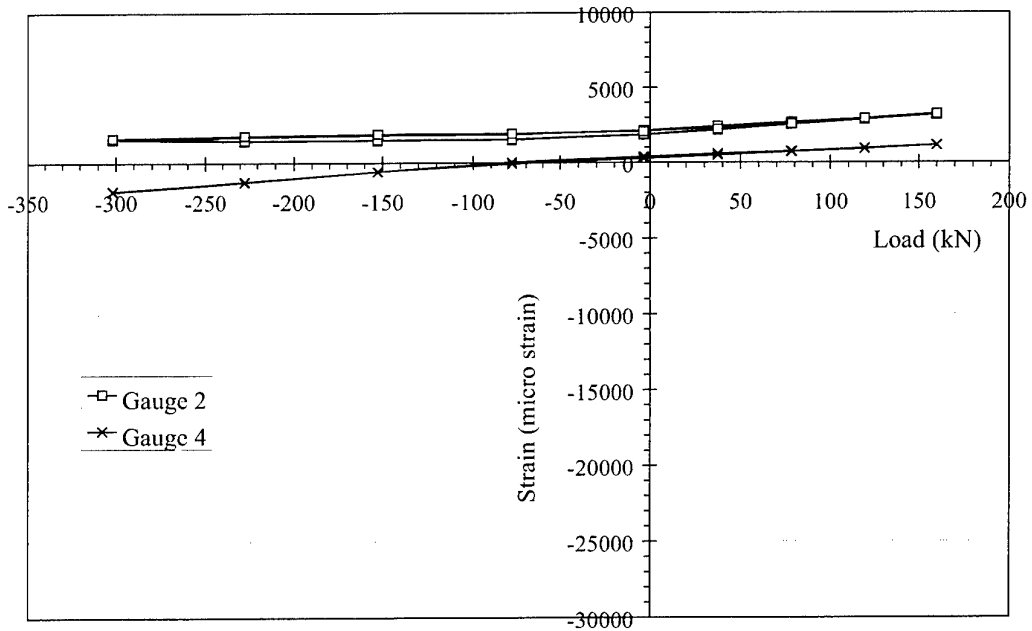


Figure A9. CPT 31 for stress-bridge specimen 1.

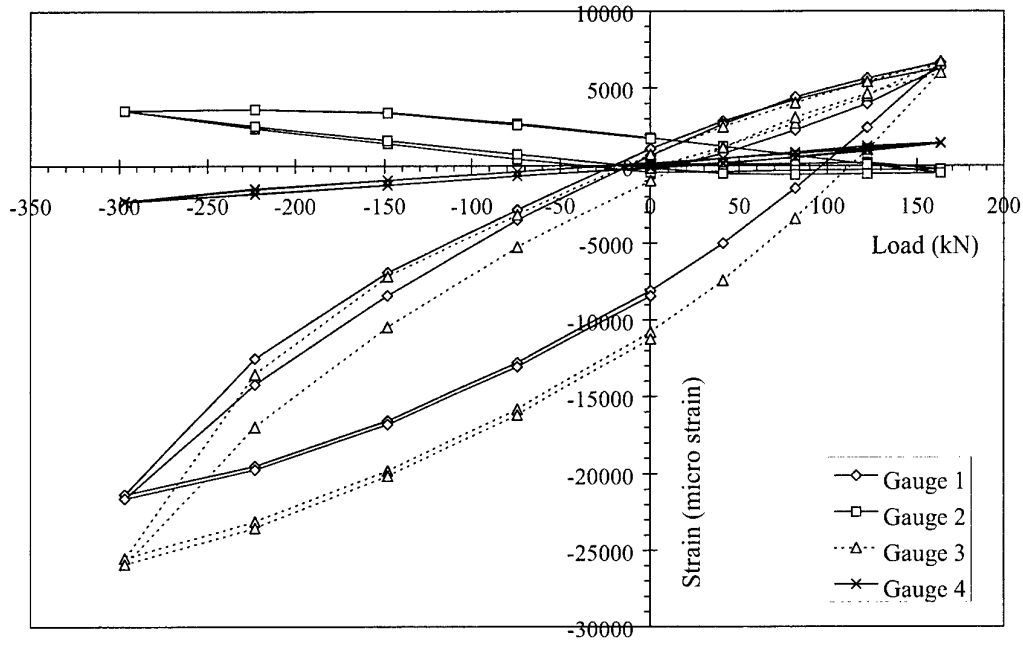


Figure A10. CPLT 1 for stress-bridge specimen 2.

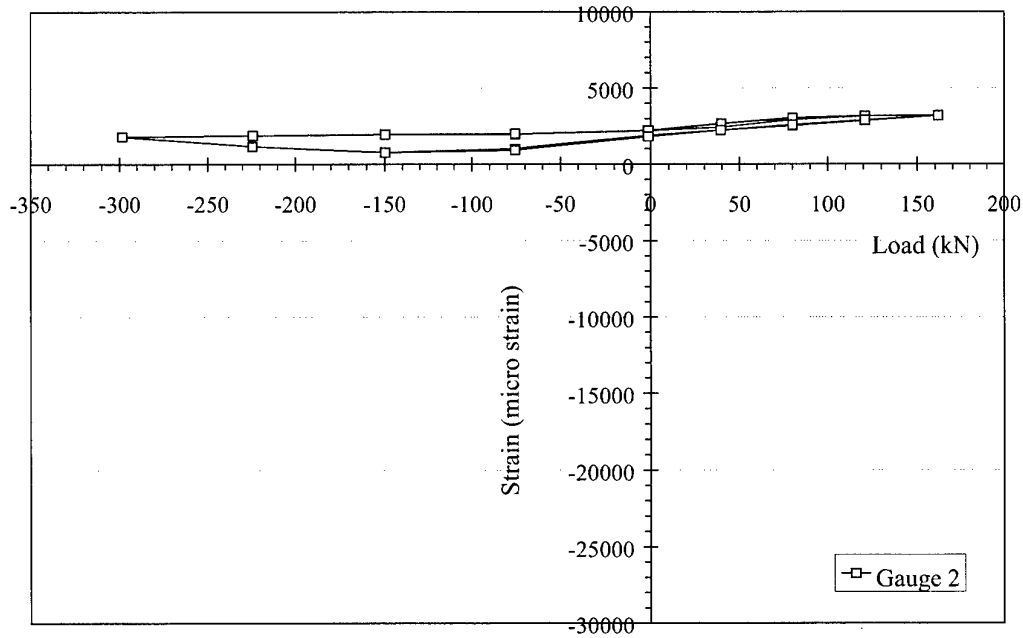


Figure A11. CPLT 31 for stress-bridge specimen 2.

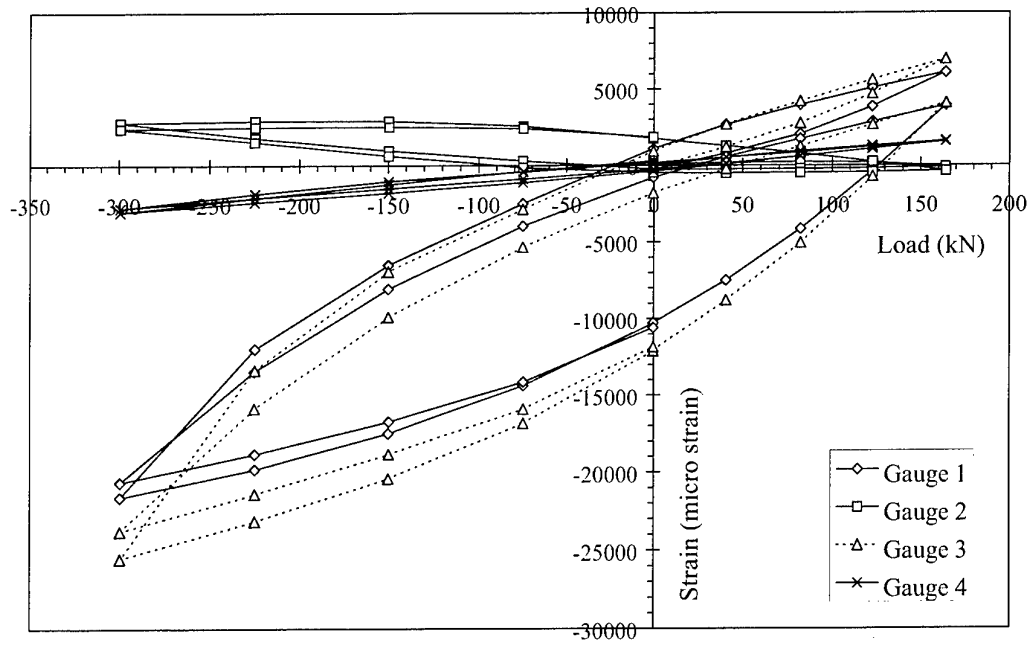


Figure A12. CPLT 1 for stress-bridge specimen 3.

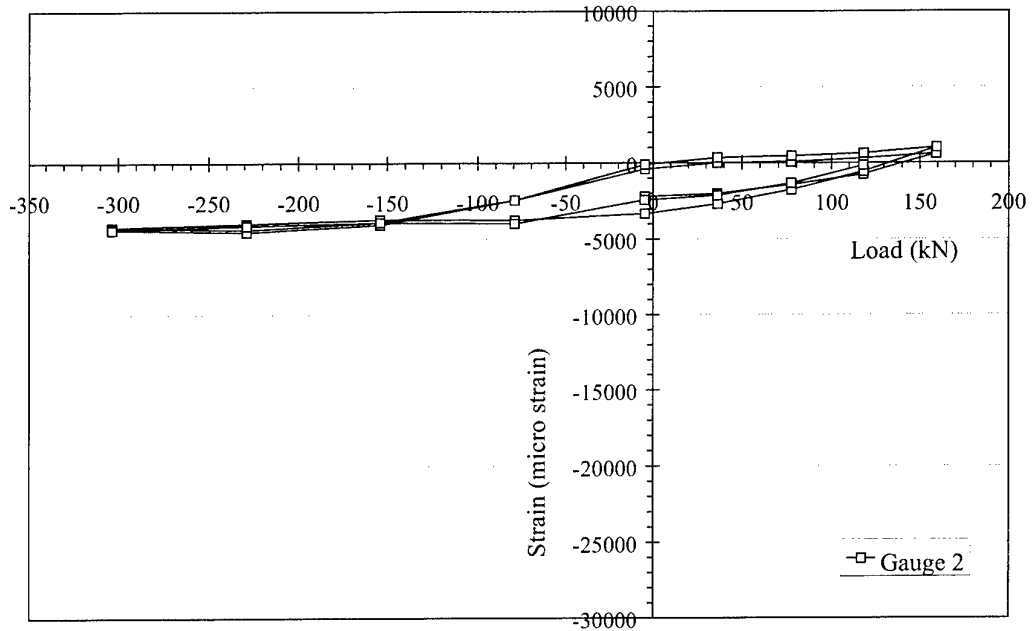


Figure A13. CPLT 31 for stress-bridge specimen 3.

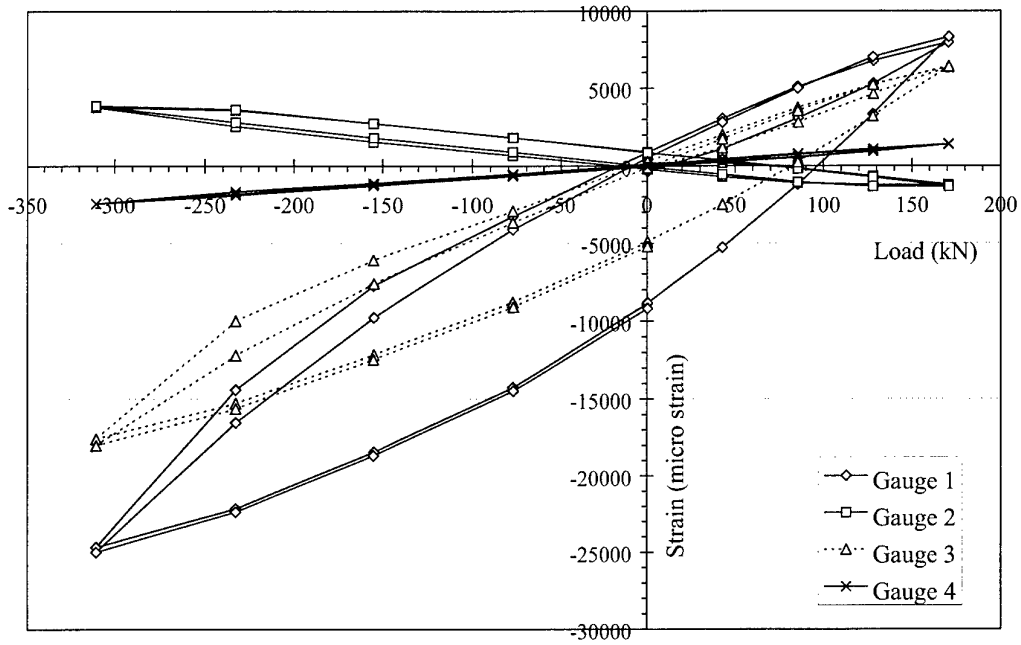


Figure A14. CPLT 1 for stress-bridge specimen 4.

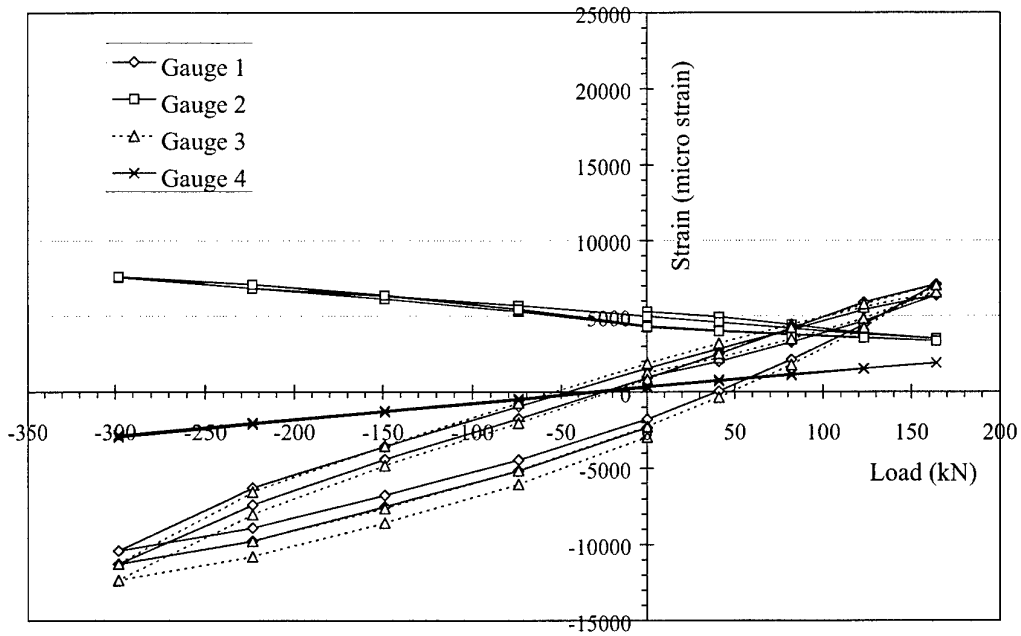


Figure A15. CPLT 1 for interference-fit plug specimen 1.

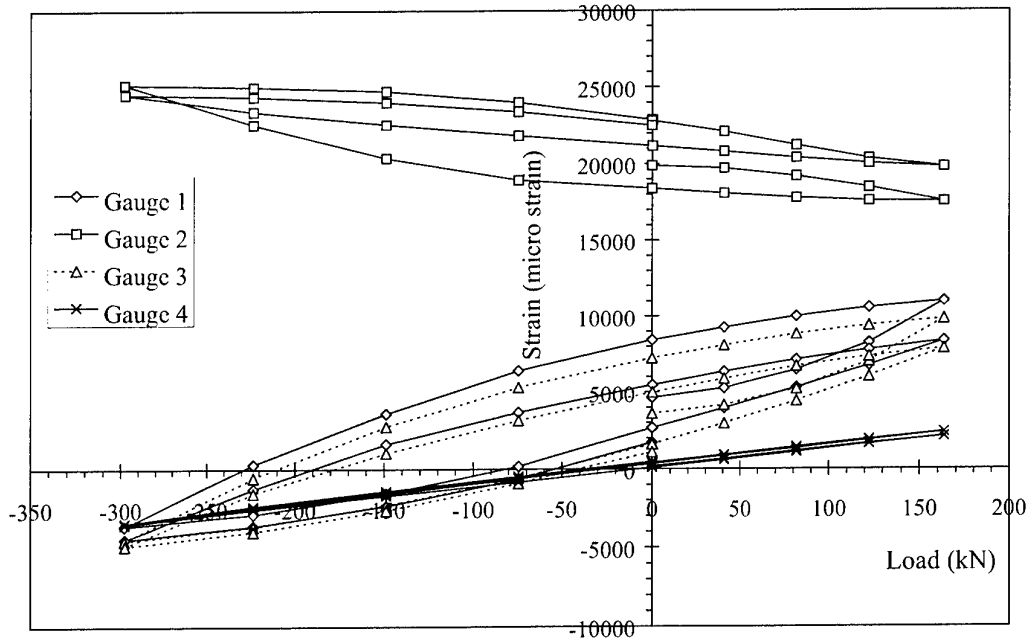


Figure A16. CPLT 1 for interference-fit plug specimen 2.

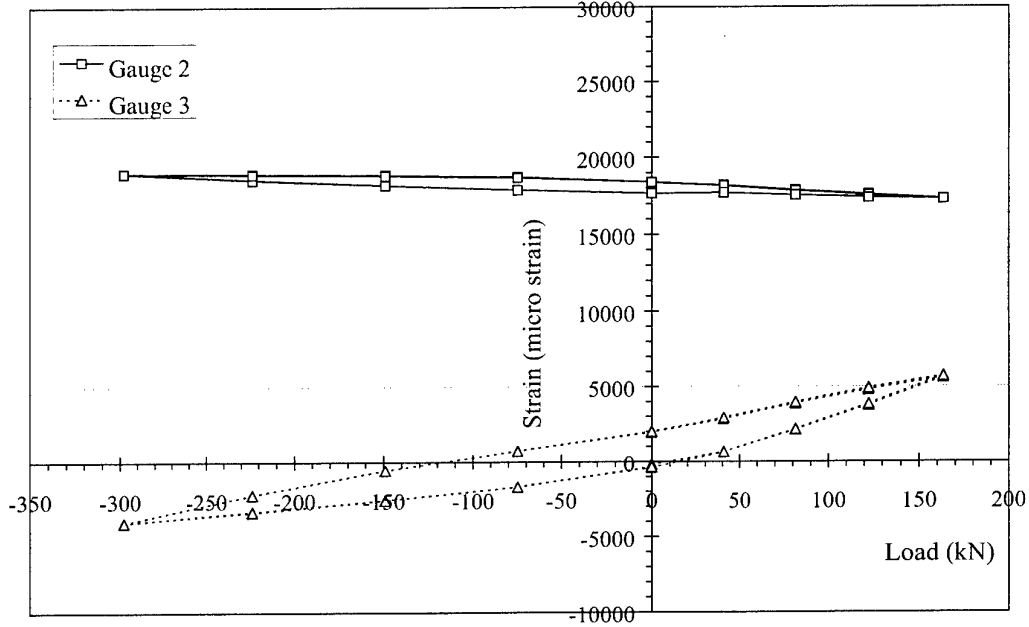


Figure A17. CPLT 31 for interference-fit plug specimen 2.

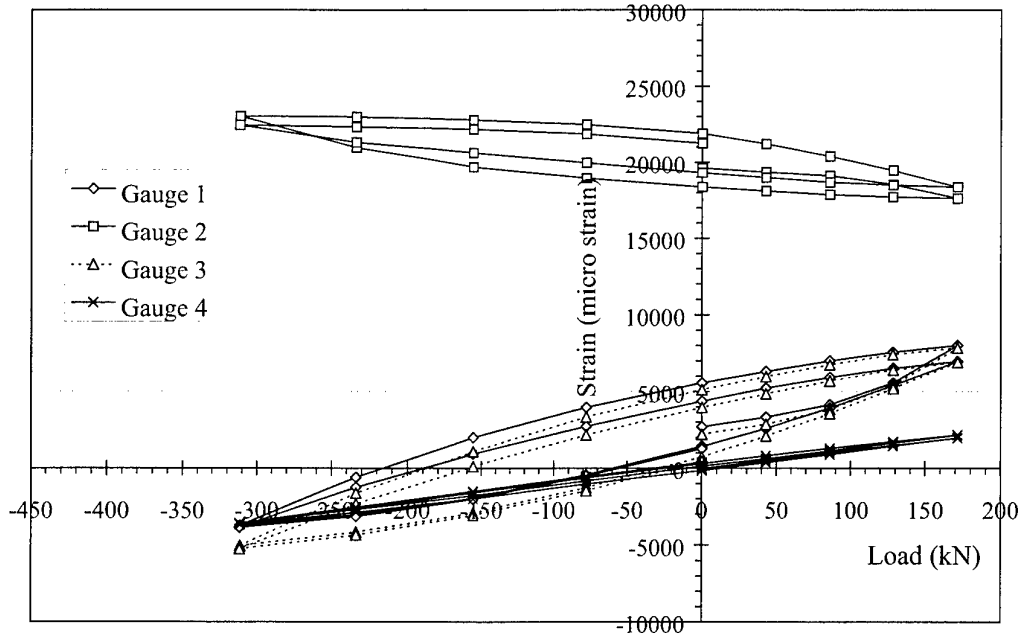


Figure A18. CPT 1 for interference-fit plug specimen 3.

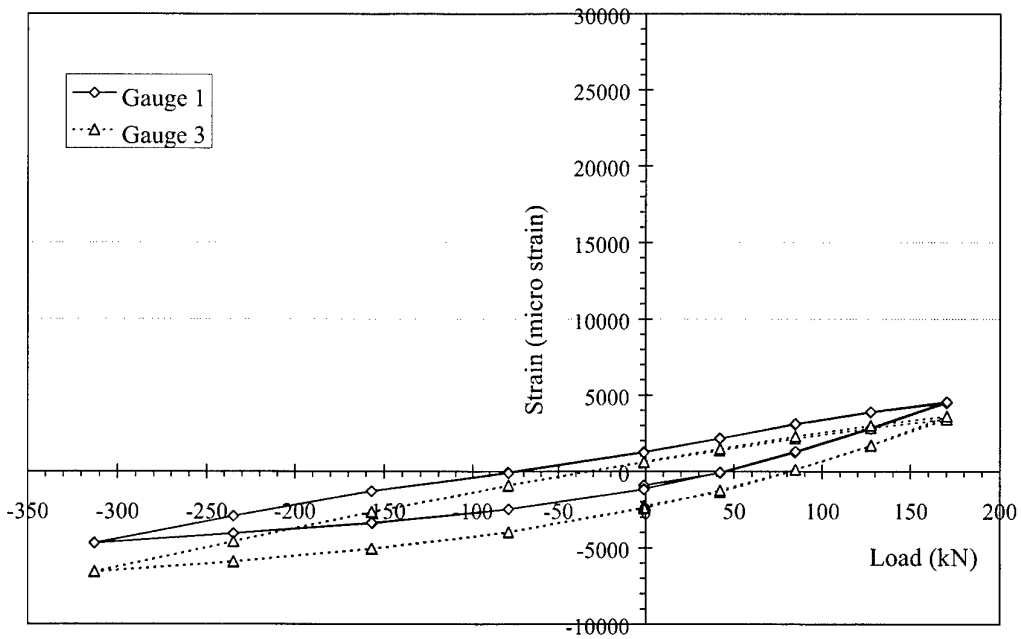


Figure A19. CPT 31 for interference-fit plug specimen 3.

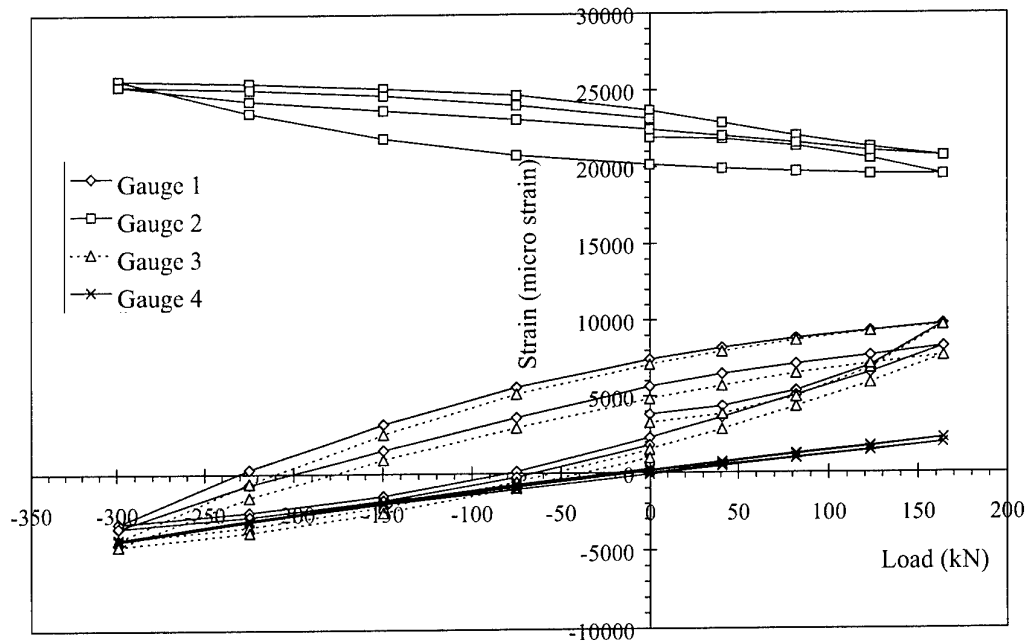


Figure A20. CPT 1 for interference-fit plug specimen 4.

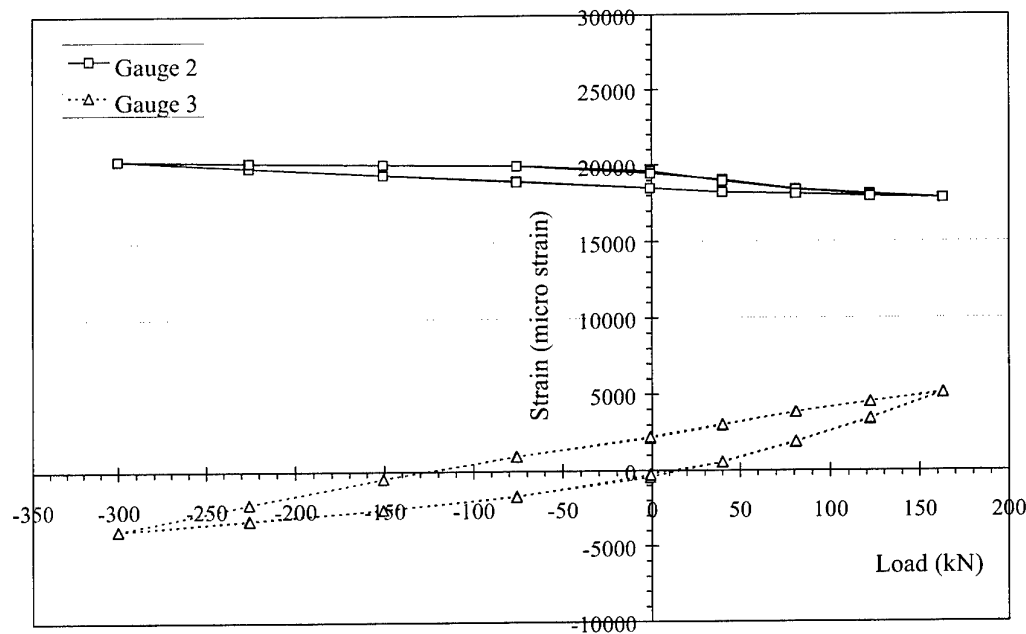


Figure A21. CPT 31 for interference-fit plug specimen 4.

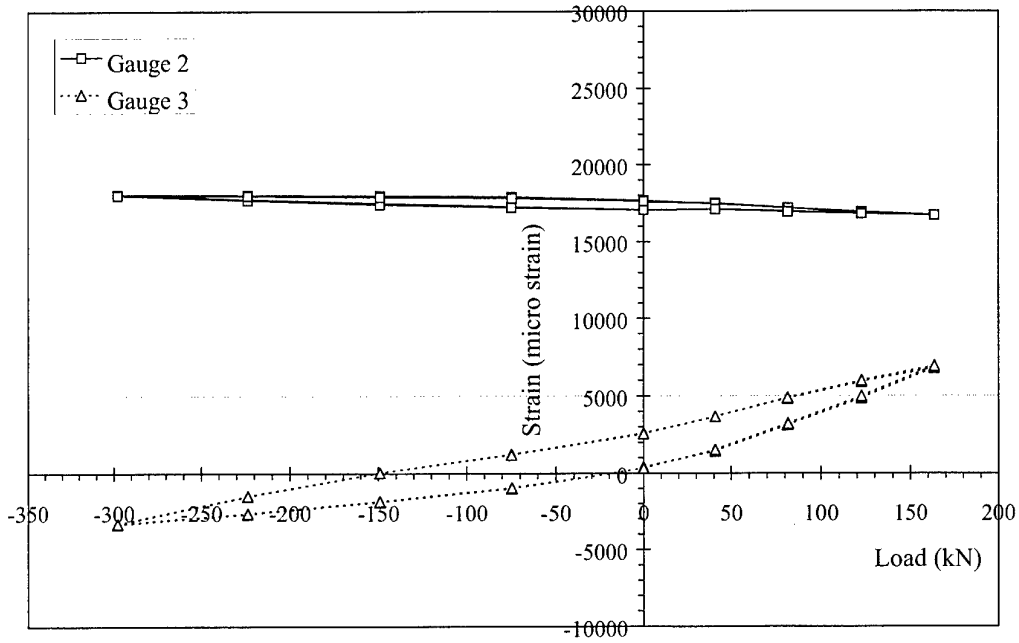


Figure A22. CPLT 69 for interference-fit plug specimen 2.

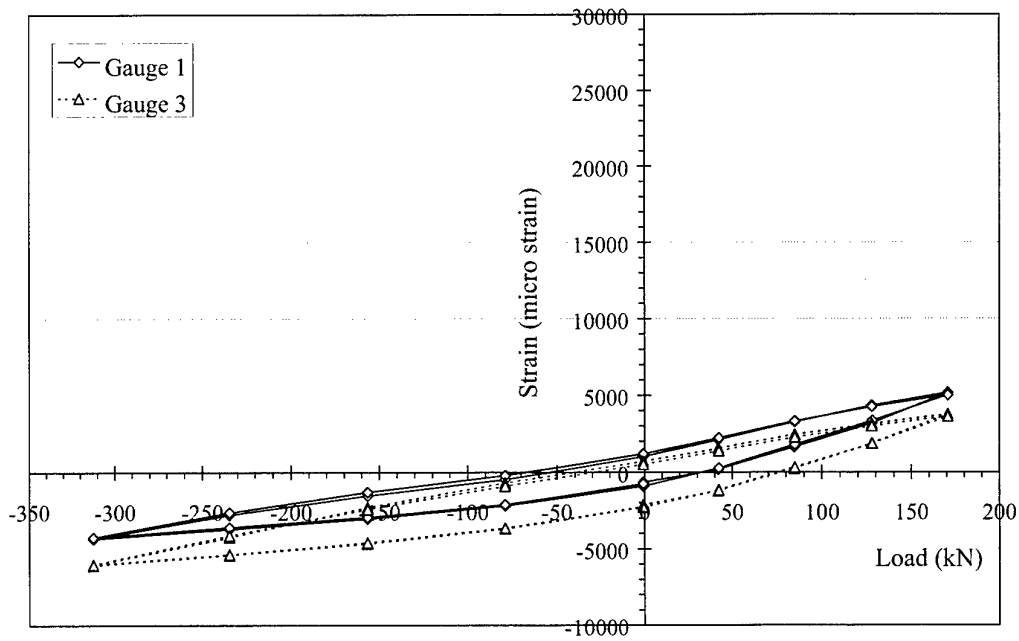


Figure A23. CPLT 69 for interference-fit plug specimen 3.

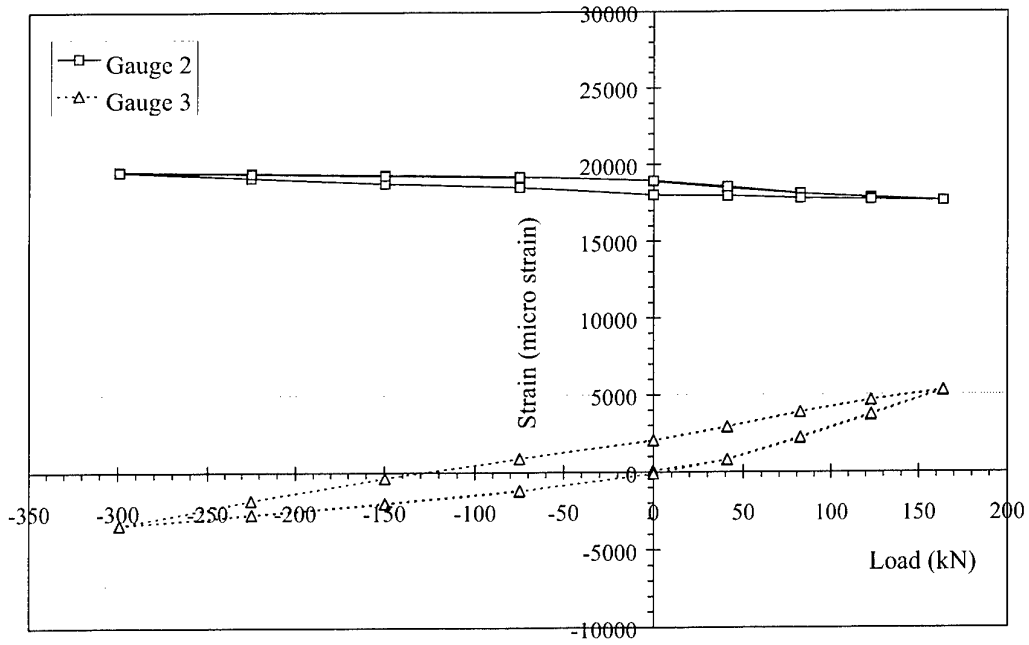


Figure A24. CPLT 69 for interference-fit plug specimen 4.

Appendix B: Raw strain-gauge data from specimen cold proof load tests

Table B1. CPLT 1 strain-gauge results for blueprint specimen 1.

Load (kN)	Gauge 1 ($\mu\epsilon$)	Gauge 2 ($\mu\epsilon$)	Gauge 3 ($\mu\epsilon$)	Gauge 4 ($\mu\epsilon$)
-0.25	7.140444	-42.0655	48.8974	-38.2271
34.425	1681.652	-470.817	1808.823	312.0949
68.975	3315.322	-891.629	3527.82	702.2261
102.9	4989.834	-1320.38	5246.817	1044.586
137.925	6705.188	-1749.13	7088.599	1394.908
102.9	4948.992	-1320.38	5287.745	1044.586
68.85	3315.322	-891.629	3568.748	702.2261
34.3	1640.81	-470.817	1808.823	312.0949
-0.25	7.140444	-42.0655	89.82586	-38.2271
-50.3	-2386.19	577.2423	-2431.37	-547.786
-100.35	-4779.51	1196.55	-4903.45	-1089.19
-150.275	-7172.84	1823.798	-7465.58	-1598.75
-200.2	-10399.3	2443.105	-11100	-2100.35
-150.275	-8087.7	1823.798	-8660.69	-1558.94
-100.225	-5694.37	1196.55	-6188.61	-1049.38
-50.3	-3301.04	577.2423	-3667.41	-547.786
-0.25	-834.2	-42.0655	-1031.62	1.58218
34.425	962.8374	-470.817	892.0244	351.9042
68.975	2882.4	-891.629	2930.264	702.2261
102.9	4793.794	-1320.38	5050.36	1044.586
137.925	6909.397	-1749.13	7366.913	1394.908
102.9	5153.201	-1320.38	5525.131	1044.586
68.85	3519.531	-891.629	3765.205	702.2261
34.3	1804.177	-470.817	2005.28	312.0949
-0.25	129.6656	-42.0655	253.5399	-38.2271
-50.3	-2345.34	577.2423	-2390.44	-547.786
-100.225	-4902.04	1196.55	-5108.09	-1049.38
-150.275	-7613.93	1823.798	-7981.27	-1598.75
-200.2	-10521.9	2443.105	-11222.8	-2100.35
-150.275	-8169.38	1823.798	-8783.47	-1558.94
-100.225	-5816.89	1196.55	-6303.21	-1049.38
-50.175	-3382.73	577.2423	-3790.2	-547.786
-0.25	-907.715	-42.0655	-1146.22	1.58218

Table B2. CPLT 1* strain-gauge results for blueprint specimen 2.

Load (kN)	Gauge 1 ($\mu\epsilon$)	Gauge 2 ($\mu\epsilon$)	Gauge 3 ($\mu\epsilon$)	Gauge 4 ($\mu\epsilon$)
0.5	40.7157	7.656963	9.17834	0.2719
-51.025	-2427.91	583.7859	-2494.25	-525.696
-99.725	-4809.78	1128.346	-4887.12	-1084.54
-95.825	-4620.49	1049.424	-4689.68	-1043.45
-148.425	-7317.84	1625.553	-7351.06	-1569.41
-194.1	-10669.8	2122.76	-10588.9	-2004.98
-204.825	-11553.1	2241.143	-11441.8	-2128.26
-216.925	-12633.7	2398.987	-12484.3	-2210.44
-222.175	-13209.4	2470.016	-13021.3	-2251.53
-228.025	-13595.9	2509.477	-13368.8	-2292.62
-229.375	-13745.7	2548.938	-13518.8	-2333.71
-227.9	-13785.2	2509.477	-13518.8	-2292.62
-227.175	-14171.6	2509.477	-13826.8	-2292.62
-226.2	-14092.8	2509.477	-13795.2	-2292.62
-170.175	-11513.7	1893.887	-11244.4	-1766.65
-149.525	-10551.5	1665.014	-10280.9	-1569.41
-118.9	-9123.96	1317.758	-8819.95	-1289.99
-119.15	-9084.53	1317.758	-8819.95	-1289.99
-98.875	-8122.31	1128.346	-7816.99	-1084.54
-49.325	-5622.14	544.325	-5305.67	-566.788
32.35	-771.644	-300.138	-488.348	361.8751
0.125	-2309.61	-31.8039	-2146.77	74.23623
0.125	-2112.42	86.5788	-2083.72	-32.6019
33.575	-456.15	-260.677	-385.808	329.0013
67.15	1696.997	-647.394	1699.066	690.6046
100.6	4165.623	-1034.11	4123.521	1093.299
134.025	6784.102	-1420.83	6705.921	1454.902
100.6	5088.4	-1034.11	5015.91	1093.299
67.15	3432.133	-686.855	3318.001	690.6046
33.575	1736.432	-339.599	1580.607	329.0013
0.125	40.7297	47.11795	-117.302	-32.6019
-58.475	-3003.65	702.1687	-3236.71	-714.717
-116.825	-6387.16	1317.759	-6593.05	-1396.83
-175.4	-10046.7	1933.348	-10336.3	-2037.86
-233.75	-14479.2	2588.399	-15003.6	-2793.94
-175.4	-11703	1933.348	-12144.8	-2037.86
-116.825	-8895.22	1317.759	-9254.42	-1355.74
-58.35	-5929.72	662.7078	-6206.08	-673.626
0.25	-2656.62	47.11795	-2857.65	-32.6019

* The full CPLT was not applied as can be seen from the load data.

Table B3. CPLT 1 strain-gauge results for blueprint specimen 3, strain gauge 3 not working.

Load (kN)	Gauge 1 ($\mu\epsilon$)	Gauge 2 ($\mu\epsilon$)	Gauge 4 ($\mu\epsilon$)
-0.75	-2.51924	11.8933	39.31796
0.25	25.4209	-1.9701	39.31796
26.1	1321.846	-448.371	270.4014
51.25	2576.36	-883.681	549.2952
75.2	3802.935	-1302.36	780.3786
100.85	5099.359	-1762.62	1051.304
124.5	6314.758	-2209.02	1282.388
134.05	6820.475	-2372.61	1362.072
125.5	6381.814	-2222.88	1322.23
100.1	5085.39	-1790.35	1091.146
75.2	3830.875	-1357.81	820.2205
50.3	2576.36	-922.499	581.1687
25.65	1335.816	-489.961	310.2434
0	67.3312	-29.6968	79.16006
-25.15	-1189.98	402.8408	-151.923
-49.8	-2416.55	849.2419	-422.849
-76.15	-3754.89	1337.233	-661.901
-101.05	-4995.43	1797.498	-932.826
-125.75	-6235.98	2271.625	-1243.59
-149.15	-7451.37	2704.163	-1474.68
-175.8	-9102.64	3206.018	-1785.44
-199.7	-10874	3652.419	-2064.34
-224.1	-12964	4126.547	-2335.26
-250.5	-15609.9	4667.218	-2606.19
-269.8	-17820	5074.802	-2837.27
-280.05	-19197.4	5304.934	-2956.8
-270.5	-18789.5	5127.483	-2877.11
-279.8	-19264.5	5291.071	-2996.64
-289.3	-20384.9	5493.476	-3076.32
-279.05	-19974.2	5318.798	-2956.8
-251.2	-18610.7	4803.08	-2685.87
-224.35	-17300.3	4328.952	-2414.95
-198.5	-16031.8	3868.688	-2096.21
-176.5	-14914.2	3477.74	-1865.13
-148.7	-13522.8	2975.886	-1594.2
-124.75	-12279.4	2529.484	-1363.12
-100.6	-10997	2096.947	-1084.23
-73.95	-9510.57	1608.956	-813.3
-49.05	-8038.12	1162.555	-582.217
-23.7	-6428.76	674.5632	-311.291
0.5	-4749.56	214.2988	-40.3659
-0.25	-927.614*	-80.4076	111.5575
40.75	1145.548*	-798.531	502.0087
81.55	3246.65*	-1513.88	932.3019
122.55	5428.779*	-2245.87	1322.753
163.55	8675.43	-3044.4	1745.078
122.55	6521.24	-2326.28	1354.627
81.55	4378.228	-1597.06	932.3019
40.75	2238.009	-865.075	541.8506
-0.25	67.05646	-121.998	111.5575
-72.75	-4051.33	1206.115	-629.503
-145.25	-8731.31	2586.908	-1402.44
-217.55	-14107	3981.565	-2183.34
-290.05	-20684.1	5442.766	-3035.96
-217.55	-17135.7	4131.289	-2223.18
-145	-13478.4	2803.177	-1482.12
-72.5	-9522.02	1477.837	-701.219
0	-4925.86	108.1344	31.87352

* Data acquisition error; amended data is presented in Figure A3.

Table B4. CPLT 1 strain-gauge results for blueprint specimen 4.

Load (kN)	Gauge 1 ($\mu\epsilon$)	Gauge 2 ($\mu\epsilon$)	Gauge 3 ($\mu\epsilon$)	Gauge 4 ($\mu\epsilon$)
0	28.47256	3.709645	-43.4401	-2.49888
25.9	1258.777	-386.501	1186.964	230.8567
50.05	2324.517	-697.076	2287.853	423.9785
75.7	3586.165	-1079.32	3518.257	665.3808
100.85	4816.469	-1429.72	4740.567	898.736
125	6038.936	-1819.93	5930.498	1132.092
149.4	7261.404	-2170.32	7233.755	1373.494
172.15	8601.416	-2560.53	8658.435	1606.85
151.6	7723.747	-2249.95	7703.251	1413.728
125	6532.625	-1859.74	6399.994	1172.326
101.55	5506.066	-1509.35	5258.632	979.204
74.7	4314.945	-1158.96	3987.754	745.8483
51.05	3241.367	-808.565	2846.392	504.4459
24.65	2097.264	-418.354	1583.608	271.0904
-0.95	913.978	-36.1077	312.7297	-37.73482
-25.65	198.781	314.2851	-869.106	-203.667
-49.05	-1311.54	664.678	-2059.04	-396.789
-74.7	-2494.82	1054.888	-3362.29	-670.379
-99.6	-3717.29	1405.281	-4665.55	-911.781
-125.95	-5018.12	1835.308	-6090.23	-1145.14
-149.9	-6209.24	2185.701	-7393.49	-1378.49
-174.8	-7541.42	2575.912	-8818.17	-1611.85
-199.7	-9038.16	2958.158	-10477.6	-1853.25
-224.6	-10911	3348.368	-12493.2	-2126.84
-249.75	-13207.1	3778.396	-14905.4	-2360.19
-275.4	-15808.7	4208.423	-17665.7	-2601.6
-295.65	-18261.5	4558.816	-20312.7	-2794.72
-276.6	-17532.7	4280.095	-19527.5	-2601.6
-249.75	-16380.8	3858.031	-18297.1	-2400.43
-223.85	-15315.1	3507.638	-17115.3	-2126.84
-198.95	-14241.5	3157.245	-15965.8	-1925.67
-174.05	-13207.1	2767.035	-14784	-1692.31
-149.9	-12133.5	2416.642	-13634.6	-1499.19
-125.75	-11067.8	2066.249	-12452.7	-1298.02
-99.35	-9837.46	1676.039	-11109	-1024.44
-76.4	-8732.54	1325.646	-9878.58	-831.313
-50.55	-7392.53	975.2534	-8421.52	-589.911
-25.85	-5974.15	593.0067	-6875.42	-356.555
0	-4406.89	162.9791	-5135.05	-123.2
42.75	-1766.04	-458.172	-2285.69	230.8568
85.45	1407.669	-1119.14	1154.587	617.1004
128.2	4894.835	-1819.93	4910.559	1011.391
170.9	8679.781	-2520.71	8941.753	1445.915
127.95	6728.536	-1899.56	6804.734	1051.624
85.45	4816.472	-1278.41	4708.19	657.3341
42.75	2865.226	-697.076	2579.266	303.2774
0	835.6171	-36.1077	401.7741	-82.9662
-77.85	-3145.24	1134.523	-3945.12	-831.313
-155.5	-7815.69	2337.007	-9004.35	-1579.66
-233.4	-13246.3	3579.309	-14897.3	-2328.01
-311.05	-20244.1	4909.209	-22522.6	-3036.12
-233.4	-16992	3738.579	-18969	-2368.24
-155.5	-13630.2	2575.912	-15253.5	-1660.13
-77.85	-9876.64	1445.098	-11141.4	-952.015
0	-5284.56	202.7965	-6163.08	-243.901

Table B5. CPLT 1 strain-gauge results for open-elongated-hole specimen 1, strain gauge 4 under test-machine grips.

Load (kN)	Gauge 1 ($\mu\epsilon$)	Gauge 2 ($\mu\epsilon$)	Gauge 3 ($\mu\epsilon$)
-0.25	0	0	0
40.3	1663.353	-298.026	1778.255
80.8	3421.595	-620.888	3586.884
121.1	5246.818	-943.749	5406.558
161.85	7429.272	-1294.21	7510.641
121.1	5684.984	-1012.74	5688.207
80.8	3965.813	-700.913	3882.339
40.05	2249.434	-391.849	2062.665
-0.5	519.1001	-82.785	256.7976
-74.2	-2695.97	510.5075	-3128.51
-147.95	-6036.63	1117.598	-6767.86
-221.95	-11241.6	1804.713	-12795.7
-295.9	-21419.9	2665.677	-25213.1
-221.95	-18899.7	2196.562	-22112.2
-147.95	-16120	1683.295	-18848.4
-74.2	-12985.9	1103.8	-15209
-0.25	-8911.22	458.077	-10583.9
40.3	-6075.7	66.228	-7427.8
80.8	-2642.95	-350.456	-3708.38
121.35	1364.731	-794.736	566.0594
161.85	5983.605	-1266.61	5420.363
121.35	4225.363	-985.142	3517.852
80.8	2442.003	-673.318	1618.101
40.3	655.8523	-378.052	-295.455
-0.25	-1144.25	-55.19	-2250.43
-74.2	-4755.63	565.6975	-6163.14
-147.95	-9101	1225.218	-10948.4
-221.95	-14512.5	1926.131	-17014.9
-295.65	-21707.3	2654.639	-25671.5
-221.95	-19198.3	2207.6	-22543
-147.95	-16432.6	1697.093	-19279.2
-74.2	-13326.4	1117.598	-15667.4
-0.25	-9374.5	471.8745	-11136.2

Table B6. CPLT 1 strain-gauge results for open-elongated-hole specimen 2, strain gauge 1 not working and 4 under test-machine grips.

Load (kN)	Gauge 2 ($\mu\epsilon$)	Gauge 3 ($\mu\epsilon$)
-0.25	40.7682	0
40.25	-277.223	1672.565
81.05	-635.982	3426.718
121.55	-986.587	5140.077
162.35	-1386.11	7212.426
121.55	-1068.12	5458.273
81.05	-709.364	3744.914
40.25	-391.373	1998.919
-0.25	-32.6142	285.5599
-74.45	644.1357	-2986.14
-148.7	1361.654	-6412.86
-222.9	2111.787	-11911.9
-296.9	3106.528	-22983.5
-222.9	2552.082	-19956.6
-148.7	1956.868	-16807.2
-74.45	1280.118	-13339.7
-0.25	521.8315	-8958.42
40.25	122.3044	-5972.28
81.05	-350.605	-2463.97
121.8	-831.668	1517.546
162.6	-1345.35	6021.234
121.8	-986.587	4226.286
81.05	-668.596	2390.544
40.25	-309.837	562.9609
-0.25	40.7682	-1313.58
-74.45	758.2863	-5017.7
-148.7	1475.805	-9594.81
-222.9	2274.859	-15330.5
-296.9	3147.296	-23301.7
-222.9	2592.85	-20274.8
-148.7	1956.868	-17166.2
-74.45	1280.118	-13698.7
-0.25	562.5996	-9399

Table B7. CPLT 1 strain-gauge results for open-elongated-hole specimen 3, strain gauge 4 under test-machine grips.

Load (kN)	Gauge 1 ($\mu\epsilon$)	Gauge 2 ($\mu\epsilon$)	Gauge 3 ($\mu\epsilon$)
0	-32.8148	0	0
42.75	1607.928	-317.991	1694.816
85.45	3330.707	-635.982	3414.596
128.2	5053.487	-994.741	5189.853
170.9	7211.063	-1394.27	7300.745
128.2	5455.469	-1076.28	5539.357
85.45	3732.689	-750.133	3805.707
42.75	2009.91	-399.527	2072.058
0	328.1485	-73.3825	327.313
-77.65	-2879.5	603.3674	-2923.63
-155.25	-6243.03	1280.117	-6352.09
-232.9	-11050.4	2030.25	-11741.7
-310.55	-20624.1	3024.991	-22684.5
-232.9	-17900.5	2511.313	-19705.4
-155.25	-15021	1916.099	-16576.5
-77.65	-11813.3	1239.349	-13109.2
0.25	-7727.9	521.8313	-8707.08
42.75	-4963.25	122.3042	-5727.98
85.7	-1681.76	-358.759	-2232.94
128.2	2083.743	-831.669	1708.685
170.9	6374.285	-1312.73	6177.34
128.2	4610.486	-994.741	4363.249
85.45	2846.688	-676.75	2546.385
42.75	1041.872	-317.991	718.4244
0	-754.741	0	-1137.27
-77.65	-4323.36	676.7499	-4848.67
-155.25	-8564.68	1394.268	-9383.9
-232.9	-13815	2193.322	-15073
-310.55	-20903.1	3065.758	-22997.9
-232.9	-18179.4	2511.313	-20004.9
-155.25	-15340.9	1916.099	-16876
-77.65	-12133.3	1280.117	-13433.7
0.25	-8170.9	562.5993	-9128.7

Table B8. CPLT 1 strain-gauge results for stress-bridge specimen 1.

Load (kN)	Gauge 1 ($\mu\epsilon$)	Gauge 2 ($\mu\epsilon$)	Gauge 3 ($\mu\epsilon$)	Gauge 4 ($\mu\epsilon$)
0	-388.682	39.95812	-317.965	39.9398
40.75	729.7706	79.91613	1120.827	471.2908
81.8	2316.228	119.8741	2869.637	862.7014
122.8	4180.316	-159.832	4809.225	1214.173
163.8	6385.491	-623.345	7098.575	1525.704
122.8	5417.752	-703.261	5699.528	1054.413
81.8	4219.977	-743.22	4228.938	623.0624
40.75	2665.249	-743.22	2440.383	239.6394
0	888.4166	-543.429	461.0497	-71.8919
-74.7	-2601.79	0	-3267.09	-663.003
-148.95	-6552.07	855.1022	-7376.8	-1206.18
-223.65	-12128.5	1909.994	-14093.8	-1717.42
-297.85	-21345.8	3276.56	-27058.8	-2180.72
-223.65	-19521.4	3356.476	-24610.5	-1365.94
-148.95	-16776.8	3236.602	-21311.6	-774.834
-74.7	-13246.9	2613.256	-17392.7	-231.651
0	-8677.92	1718.196	-12194	311.5311
40.75	-5616.06	1166.775	-8585.06	591.1105
81.8	-1983.07	543.4294	-4276.63	902.6414
122.55	2086.192	-79.9162	580.2867	1214.173
163.8	6615.528	-743.22	5938.002	1525.704
122.8	5647.789	-823.136	4499.209	1054.413
81.8	4410.352	-863.094	2909.382	591.1105
40.75	2744.572	-863.094	1001.59	239.6394
0	848.7546	-583.387	-1128.78	-71.8919
-74.7	-3141.19	151.8406	-5437.21	-623.063
-148.95	-7979.88	1094.85	-10914.2	-1166.25
-223.65	-13905.3	2141.751	-17893.5	-1717.42
-297.85	-21536.2	3316.518	-27599.4	-2180.72
-223.65	-19719.7	3396.434	-25119.3	-1397.9
-148.95	-16927.5	3276.56	-21780.6	-774.834
-74.7	-13365.9	2653.214	-17822	-231.651
0	-8796.91	1758.154	-12694.8	311.5311

Table B9. CPLT 31 strain-gauge results for stress-bridge specimen 1, strain gauges 1 and 3 not working.

Load (kN)	Gauge 2 ($\mu\epsilon$)	Gauge 4 ($\mu\epsilon$)
-3.65	2061.835	271.5913
37.35	2341.542	471.2909
78.1	2613.256	702.9423
119.15	2884.971	894.6538
159.9	3156.686	1134.293
119.15	2845.013	934.5937
78.1	2533.34	742.8821
37.35	2141.751	583.1226
-3.65	1830.078	391.411
-78.1	1518.406	0
-152.85	1478.448	-583.123
-227.55	1438.49	-1286.07
-301.75	1558.364	-1909.13
-227.3	1710.204	-1246.13
-152.85	1830.078	-583.123
-78.1	1870.036	-79.8798
-3.4	2141.751	271.5913
37.35	2413.466	471.2909
78.35	2693.172	702.9423
119.15	2924.929	934.5937
160.15	3236.602	1134.293
119.15	2924.929	934.5937
78.35	2573.298	742.8821
37.35	2221.667	583.1226
-3.4	1870.036	391.411
-78.1	1558.364	39.93987
-152.85	1518.406	-583.123
-227.3	1478.448	-1286.07
-301.75	1638.28	-1869.19
-227.3	1790.12	-1246.13
-152.6	1909.995	-583.123
-78.1	1949.953	-79.8798
-3.65	2061.835	271.5913

Table B10. CPLT 1 strain-gauge results for stress-bridge specimen 2.

Load (kN)	Gauge 1 ($\mu\epsilon$)	Gauge 2 ($\mu\epsilon$)	Gauge 3 ($\mu\epsilon$)	Gauge 4 ($\mu\epsilon$)
0.25	-307.592	78.9865	-144.809	0
40.8	772.9248	118.4798	1188.958	461.0306
81.8	2271.452	118.4798	2720.884	850.5218
122.3	3967.154	189.5677	4466.213	1240.014
163.35	6317.475	-229.061	6737.428	1470.529
122.3	5355.263	-268.555	5396.04	1009.498
81.8	4235.311	-308.048	4024.165	540.5186
40.8	2847.202	-387.035	2492.238	111.2832
0.25	1080.517	-426.528	708.8022	-158.976
-74.2	-2847.2	426.5275	-3162.93	-659.751
-148.2	-6893.22	1429.657	-7141.37	-1247.96
-222.65	-12516.6	2393.294	-13543.5	-1828.23
-296.85	-21334.3	3546.498	-25494	-2289.26
-222.65	-19488.7	3625.485	-23108.5	-1478.48
-148.2	-16562.7	3428.018	-19793.1	-930.01
-74.2	-12784.8	2701.342	-15814.7	-389.491
0.25	-8084.16	1777.198	-10792.1	151.0272
40.8	-5008.24	1232.191	-7408.12	461.0306
81.8	-1466.98	655.5886	-3422.06	771.034
122.3	2429.192	78.9865	1044.149	1081.038
163.35	6664.502	-466.021	5990.519	1430.785
122.3	5623.421	-537.109	4618.644	930.0098
81.8	4393.051	-576.602	3086.718	500.7746
40.8	2657.914	-505.514	1158.472	190.7712
0.25	654.6198	-157.973	-967.934	-119.232
-74.2	-3501.82	734.5753	-5243.61	-659.751
-148.45	-8399.64	1619.225	-10456.7	-1247.96
-222.65	-14212.3	2543.368	-16965.5	-1788.48
-296.85	-21602.5	3546.498	-25897.9	-2329
-222.65	-19717.5	3625.485	-23520	-1518.22
-148.2	-16791.4	3396.424	-20128.4	-930.01
-74.2	-13053	2622.355	-16188.1	-389.491
0.25	-8431.19	1737.705	-11234.1	190.7712

Table B11. CPLT 31 strain-gauge results for stress-bridge specimen 2, strain gauges 1, 3 and 4 not working.

Load (kN)	Gauge 2 ($\mu\epsilon$)
-1.45	2203.726
39.3	2432.787
80.1	2930.403
120.85	3167.363
161.65	3198.957
120.85	2859.315
80.1	2543.368
39.3	2235.321
-1.45	1887.78
-75.7	1003.13
-149.9	774.0687
-224.35	1161.103
-298.35	1816.692
-224.1	1887.78
-149.9	1966.766
-75.7	1966.766
-1.2	2203.726
39.55	2661.848
80.1	3048.883
120.85	3167.363
161.65	3198.957
120.85	2890.909
80.1	2582.862
39.3	2235.321
-1.2	1816.692
-75.7	924.1432
-149.9	774.0687
-224.35	1161.103
-298.35	1816.692
-224.1	1887.78
-149.9	1966.766
-75.7	2006.26

Table B12. CPLT 1 strain-gauge results for stress-bridge specimen 3.

Load (kN)	Gauge 1 ($\mu\epsilon$)	Gauge 2 ($\mu\epsilon$)	Gauge 3 ($\mu\epsilon$)	Gauge 4 ($\mu\epsilon$)
-0.25	-267.938	114.9009	-157.945	39.74424
40.75	772.2897	153.2012	1192.485	508.7235
81.8	2041.052	222.1416	2771.934	930.01
122.8	3853.57	191.5015	4698.862	1279.757
164.05	6083.756	-114.901	6973.27	1550.017
122.8	5082.93	-183.841	5622.841	1088.986
81.8	3963.898	-222.142	4201.336	580.2627
40.75	2655.733	-260.442	2692.962	119.2321
-0.25	1079.63	-260.442	923.978	-270.259
-75.2	-2498.12	298.7422	-2858.8	-890.266
-149.9	-6501.42	972.8268	-6902.2	-1510.27
-224.6	-11962.6	1792.453	-13346.4	-2138.23
-299.3	-21624.1	2803.58	-25531.8	-2797.98
-224.6	-19811.6	2918.481	-23138.9	-1860.02
-149.9	-17471.1	2918.481	-20398.6	-1049.24
-74.95	-14350.4	2581.439	-16813.2	-429.235
-0.25	-10307.7	1761.813	-12114.4	158.9761
40.75	-7502.25	1271.569	-8797.53	508.7235
82.05	-4153.03	788.9857	-5054.24	850.522
123.05	-346.743	222.1416	-734.444	1240.013
164.3	3924.495	-375.343	4082.877	1589.761
123.05	2852.745	-444.283	2692.962	1088.986
81.8	1733.713	-482.583	1231.971	580.2627
40.75	543.7547	-520.884	-236.917	79.48824
-0.25	-803.813	-482.583	-1816.37	-389.491
-75.2	-3963.9	-145.541	-5322.75	-1128.73
-149.9	-8038.12	635.7847	-9871.56	-1788.48
-224.85	-13428.4	1532.011	-15849.8	-2408.49
-299.3	-20662.7	2397.597	-23794.4	-3068.24
-224.6	-18810.8	2504.838	-21401.5	-2138.23
-149.65	-16698.8	2543.138	-18819.1	-1240.01
-74.95	-14121.9	2428.238	-15889.3	-389.491
-0.25	-10583.5	1830.753	-11838	270.2594

Table B13. CPLT 31 strain-gauge results for stress-bridge specimen 3, strain gauges 1, 3 and 4 not working.

Load (kN)	Gauge 2 ($\mu\epsilon$)
-4.65	-2206.1
36.35	-2022.26
77.4	-1424.77
118.15	-750.686
159.15	597.4843
118.15	298.7421
77.15	68.94041
36.35	0
-4.65	-413.643
-79.35	-2435.9
-154.05	-3891.31
-228.75	-4381.55
-303.25	-4228.35
-228.75	-3967.91
-154.05	-3707.47
-79.35	-3745.77
-4.65	-3332.12
36.6	-2696.34
77.4	-1761.81
118.4	-566.844
159.4	1011.127
118.4	635.7845
77.4	444.2832
36.35	337.0424
-4.65	-114.901
-79.35	-2435.9
-154.05	-4044.51
-228.75	-4527.09
-303.25	-4381.55
-228.75	-4113.45
-154.05	-3891.31
-79.35	-3967.91
-4.9	-2435.9

Table B14. CPLT 1 strain-gauge results for stress-bridge specimen 4.

Load (kN)	Gauge 1 ($\mu\epsilon$)	Gauge 2 ($\mu\epsilon$)	Gauge 3 ($\mu\epsilon$)	Gauge 4 ($\mu\epsilon$)
0.25	-360.394	190.1035	-189.534	39.7441
42.75	1081.182	190.1035	1160.896	429.2356
85.7	3079.729	-144.479	2819.318	778.9829
128.2	5274.855	-669.165	4627.787	1088.987
170.65	7953.237	-1224.27	6365.182	1398.99
128.2	6757.384	-1224.27	5243.773	930.0098
85.45	5078.277	-1110.2	3743.296	540.5188
42.75	3038.776	-707.185	2005.901	230.5154
0.25	876.413	-220.52	276.4039	-79.4879
-77.65	-3284.5	669.1643	-2929.88	-659.751
-155.25	-7756.66	1558.849	-6088.78	-1279.76
-232.9	-14399.4	2562.595	-9982.12	-1899.76
-310.55	-24678.8	3786.862	-17579.3	-2448.23
-232.9	-22156	3604.363	-15265.4	-1669.25
-155	-18437.4	2745.095	-12146	-1128.73
-77.65	-14276.5	1817.389	-8789.64	-540.519
0.25	-8878.79	889.6843	-4935.78	39.7441
42.75	-5283.05	372.6029	-2503.43	389.4915
85.45	-1204.04	-182.499	236.9177	739.2389
127.95	3317.262	-737.602	3206.283	1049.243
170.9	8313.63	-1338.33	6404.668	1398.99
127.95	6994.916	-1338.33	5212.184	930.0098
85.45	4996.369	-1041.77	3553.762	580.2628
42.75	2801.243	-555.102	1737.395	270.2594
0.25	516.0188	-76.0415	-110.561	0
-77.65	-4119.96	889.6843	-3664.32	-620.007
-155	-9763.4	1817.389	-7597.15	-1200.27
-232.9	-16520.8	2821.136	-12185.5	-1820.28
-310.55	-24998.2	3862.903	-18005.7	-2448.23
-232.9	-22360.8	3642.384	-15612.9	-1669.25
-155.25	-18675	2745.095	-12454	-1128.73
-77.4	-14481.3	1817.389	-9097.63	-540.519
0.25	-9198.23	851.6643	-5204.29	79.4881

Table B15. CPLT 1 strain-gauge results for interference-fit plug specimen 1.

Load (kN)	Gauge 1 ($\mu\epsilon$)	Gauge 2 ($\mu\epsilon$)	Gauge 3 ($\mu\epsilon$)	Gauge 4 ($\mu\epsilon$)
0.25	993.2707	5299.849	1272.781	309.4941
41	1986.541	4941.09	2227.367	738.0243
82.05	3256.625	4419.259	3467.513	1126.876
122.8	4648.832	3864.813	4821.882	1515.727
164.05	6358.561	3506.054	6567.877	1896.643
123.05	5405.998	3783.277	5572.497	1515.727
82.05	4095.206	4182.804	4422.099	1126.876
41	2825.122	4582.331	3181.953	698.3456
0.25	1546.897	4981.858	1868.377	309.4941
-74.45	-952.563	5699.376	-717.979	-428.53
-148.9	-3582.29	6335.358	-3549.1	-1237.98
-223.65	-6285.29	6849.036	-6535.24	-2055.36
-298.1	-10413.1	7566.554	-11275.5	-2983.84
-223.65	-8906.87	7093.644	-9766.15	-2126.78
-148.9	-6757.5	6335.358	-7612.21	-1317.33
-74.45	-4453.44	5454.768	-5140.08	-539.631
0.25	-1791.14	4345.876	-2276.32	269.8154
41	40.70731	4027.885	-358.99	698.3456
82.05	2108.665	3783.277	1786.789	1087.197
123.05	4412.727	3587.59	4218.127	1515.727
164.05	7075.018	3351.135	7049.25	1896.643
123.05	5886.35	3546.822	5776.468	1515.727
82.05	4176.622	3742.509	4218.127	1166.555
41	2499.46	3987.117	2504.768	777.7031
0.25	911.8546	4264.34	832.2031	388.8515
-74.45	-1750.44	5299.849	-2031.55	-428.53
-148.9	-4412.73	6131.518	-4821.88	-1237.98
-223.65	-7392.54	6849.036	-8011.99	-2055.36
-298.1	-11292.3	7607.322	-12352.5	-2825.13
-223.65	-9778.02	7093.644	-10794.2	-2015.68
-148.9	-7514.66	6376.126	-8566.8	-1237.98
-74.45	-5169.89	5454.768	-6053.87	-460.273
0.25	-2344.77	4305.108	-2953.51	309.4941

Table B16. CPLT 1 strain-gauge results for interference-fit plug specimen 2.

Load (kN)	Gauge 1 ($\mu\epsilon$)	Gauge 2 ($\mu\epsilon$)	Gauge 3 ($\mu\epsilon$)	Gauge 4 ($\mu\epsilon$)
0	4643.998	19881.85	3601.708	166.0424
40.75	5263.764	19716.99	4158.335	647.5649
81.8	6469.336	19197.69	5238.848	1178.9
122.55	8252.223	18472.32	7031.516	1660.423
163.55	10985.98	17540.87	9831.025	2108.737
122.55	10569.98	17582.09	9397.184	1627.214
81.8	9992.662	17788.16	8832.37	1095.879
40.75	9245.546	18068.42	8071.1	572.8459
0	8422.022	18389.89	7236.159	83.02118
-74.45	6426.886	18950.41	5320.705	-846.816
-148.95	3608.225	20401.15	2758.581	-1701.93
-223.4	297.1483	22577.28	-556.628	-2590.26
-297.85	-3642.19	25190.27	-4559.44	-3528.4
-223.4	-2895.07	25033.66	-3675.38	-2474.03
-148.95	-1570.64	24745.16	-2316.55	-1494.38
-74.45	169.7993	24028.03	-597.556	-523.033
0	2657.352	22816.32	1596.211	406.8036
40.75	3939.333	22090.95	2955.038	896.6283
81.8	5306.214	21208.96	4436.649	1419.661
122.55	6757.993	20359.94	6032.861	1909.486
163.55	8379.572	19799.42	7874.643	2391.009
122.55	7793.766	20038.47	7358.944	1867.975
81.8	7131.551	20401.15	6712.274	1336.64
40.75	6341.987	20805.05	5877.333	855.1177
0.25	5476.013	21167.74	4993.277	323.7825
-74.45	3693.125	21851.9	3159.68	-606.054
-148.95	1621.579	22577.28	1039.584	-1577.4
-223.4	-1281.98	23418.05	-1555.28	-2515.54
-297.6	-4474.2	24547.33	-4878.68	-3445.38
-223.4	-3642.19	24390.71	-3994.62	-2391.01
-148.95	-2360.2	24028.03	-2635.8	-1419.66
-74.45	-662.215	23418.05	-916.798	-481.523
0	1706.479	22494.85	1080.512	448.3141

Table B17. CPLT 31 strain-gauge results for interference-fit plug specimen 2, strain gauges 1 and 4 not working.

Load (kN)	Gauge 2 ($\mu\epsilon$)	Gauge 3 ($\mu\epsilon$)
0	18348.68	-196.4568
40.75	18192.06	638.4846
81.55	17870.59	2120.096
122.55	17582.09	3757.236
163.35	17301.83	5599.019
122.3	17425.47	4796.82
81.55	17540.87	3880.022
40.55	17705.73	2840.438
0	17664.52	1956.382
-74.7	17903.56	720.3416
-149.15	18225.03	-556.6276
-223.65	18587.72	-2193.768
-297.85	18991.62	-4035.55
-223.65	18950.41	-3356.137
-149.15	18876.22	-2553.938
-74.7	18752.58	-1678.068
0	18389.89	-401.0993
40.75	18150.84	638.4846
81.55	17829.37	2161.025
122.55	17540.87	3839.093
163.35	17301.83	5713.619
122.55	17384.26	4919.605
81.55	17540.87	3961.879
40.75	17705.73	2922.295
0	17664.52	17903.56
-149.15	18225.03	-556.6276
-223.65	18554.75	-2193.768
-297.85	18991.62	-4035.55
-223.65	18909.19	-3315.208
-149.15	18835.01	-2553.938
-74.7	18711.36	-1678.068
0	18389.89	-360.1708

Table B18. CPLT 1 strain-gauge results for interference-fit plug specimen 3.

Load (kN)	Gauge 1 ($\mu\epsilon$)	Gauge 2 ($\mu\epsilon$)	Gauge 3 ($\mu\epsilon$)	Gauge 4 ($\mu\epsilon$)
0.25	2710.666	19602.72	2212.194	-32.8731
42.95	3340.877	19332.34	2872.669	484.877
85.95	4153.318	19101.72	3843.488	1010.845
128.65	5565.598	18521.19	5395.208	1487.504
171.4	8010.512	17622.57	7846.127	1972.381
128.4	7562.531	17702.09	7416.421	1446.413
85.95	7008.249	17861.14	6755.945	887.5717
42.95	6302.109	18091.76	5984.065	361.6032
0.25	5565.598	18362.14	5124.651	-156.147
-77.85	3971.088	18942.67	3342.164	-1035.5
-155.75	2004.526	19682.25	1082.224	-2005.25
-233.65	-592.246	20962.58	-1631.29	-2884.61
-311.25	-3743.3	23022.26	-5053.03	-3690
-233.65	-3037.16	22982.5	-4161.79	-2605.19
-155.75	-1966.56	22791.64	-2920.42	-1602.56
-77.85	-440.388	22481.5	-1281.16	-641.024
0.25	1412.28	21893.02	732.093	287.6389
42.95	2596.773	21201.16	2092.831	805.389
85.95	3933.124	20382.06	3572.932	1290.266
128.65	5413.74	19451.63	5204.227	1725.834
171.4	6970.285	18362.14	6915.096	2169.62
128.65	6522.303	18481.43	6405.814	1651.87
85.95	5930.057	18672.29	5705.551	1125.901
42.95	5231.51	18982.43	4854.095	608.1509
0.25	4373.512	19292.58	3962.851	123.2737
-77.85	2741.038	19952.63	2172.406	-838.262
-155.75	926.3341	20612.68	111.4055	-1799.8
-233.65	-1260.42	21312.49	-2331.56	-2687.37
-311.5	-3857.2	22441.74	-5251.97	-3607.81
-233.65	-3151.06	22322.45	-4352.77	-2564.1
-155.75	-2034.9	22171.35	-3071.61	-1520.38
-77.85	-516.317	21861.21	-1480.1	-558.841
0.25	1260.422	21232.97	461.5369	361.6032

Table B19. CPLT 31 strain-gauge results for interference-fit plug specimen 3, strain gauges 2 and 4 not working.

Load (kN)	Gauge 1 ($\mu\epsilon$)	Gauge 3 ($\mu\epsilon$)
-0.95	-926.3342	-2259.939
42	-113.8935	-1360.738
84.5	1222.457	71.6178
127.45	2779.002	1671.082
170.15	4487.406	3413.781
127.45	3857.195	2832.882
84.5	3075.126	2132.619
41.75	2148.792	1360.738
-0.95	1260.422	580.8999
-79.1	-75.92902	-938.9888
-157	-1298.386	-2681.688
-234.85	-2930.861	-4623.326
-312.75	-4707.6	-6604.752
-234.85	-4077.389	-5944.277
-156.75	-3409.213	-5092.821
-78.85	-2482.879	-4002.639
-0.95	-1184.493	-2411.132
42	-75.92902	-1249.333
84.7	1298.386	111.4055
127.7	2854.931	1702.912
170.4	4563.335	3612.72
127.45	3895.159	2992.032
84.7	3113.09	2291.77
42	2148.792	1472.144
-0.95	1222.457	620.6876
-78.85	-113.8935	-899.2012
-157	-1298.386	-2641.901
-234.85	-2930.861	-4591.496
-312.75	-4707.6	-6572.922
-234.85	-4077.389	-5912.447
-157	-3371.249	-5053.033
-78.85	-2482.879	-3962.851
-0.95	-1184.493	-2371.345

Table B20. CPLT 1 strain-gauge results for interference-fit plug specimen 4.

Load (kN)	Gauge 1 ($\mu\epsilon$)	Gauge 2 ($\mu\epsilon$)	Gauge 3 ($\mu\epsilon$)	Gauge 4 ($\mu\epsilon$)
-0.25	3811.984	21937.79	3258.033	-31.5886
41	4346.85	21826.63	3827.158	505.4166
82.05	5348.663	21358.18	4948.911	971.3473
123.05	7004.202	20548.31	6845.994	1468.867
164.05	9737.963	19500.26	9666.873	1934.797
123.05	9287.997	19539.95	9262.713	1429.381
82.05	8787.09	19690.81	8660.595	931.8617
40.75	8167.324	19889.31	7934.755	426.4451
-0.25	7420.209	20159.26	7085.191	-110.56
-74.95	5637.322	20818.27	5196.357	-1034.53
-149.65	3234.668	21937.79	2573.434	-1966.39
-224.6	288.6583	23605.15	-610.366	-3040.4
-299.05	-3192.22	25740.97	-4231.32	-4311.83
-224.6	-2487.55	25542.48	-3423	-3079.88
-149.65	-1451.78	25193.12	-2136.28	-1887.42
-74.95	118.8595	24732.61	-569.125	-844.993
-0.25	2275.304	23684.55	1484.673	157.9427
40.75	3608.225	22866.75	2820.879	694.9477
82.05	5051.515	22017.19	4305.553	1239.85
123.05	6545.745	21278.78	5880.956	1737.369
164.3	8243.733	20699.17	7646.068	2242.786
123.05	7666.417	21048.53	7126.432	1697.884
82.05	7089.101	21548.73	6483.074	1200.364
40.75	6460.846	22017.19	5674.752	655.462
-0.25	5637.322	22445.94	4833.437	118.4569
-74.95	3642.185	23144.64	2977.595	-884.479
-149.65	1528.19	23763.95	923.7968	-1887.42
-224.6	-704.665	24383.26	-1534.16	-2969.32
-299.05	-3480.88	25351.92	-4635.48	-4201.28
-224.35	-2776.21	25121.66	-3785.92	-2969.32
-149.65	-1740.44	24732.61	-2499.2	-1808.44
-74.95	-254.698	24073.61	-932.045	-726.536
-0.25	1782.888	23144.64	965.0378	236.914

Table B21. CPLT 31 strain-gauge results for interference-fit plug specimen 4, strain gauges 1 and 4 not working.

Load (kN)	Gauge 2 ($\mu\epsilon$)	Gauge 3 ($\mu\epsilon$)
-1	19460.55	-247.4456
40.05	19031.8	519.6357
80.8	18412.5	1847.594
121.85	18102.84	3381.756
162.85	17832.89	5072.634
121.85	17983.75	4503.509
80.8	18102.84	3818.91
40.05	18221.94	2977.595
-1	18491.89	2128.032
-75.95	18992.11	965.0377
-150.65	19420.86	-486.6429
-225.6	19889.31	-2177.521
-300.05	20389.52	-3909.64
-225.6	20230.72	-3225.041
-150.65	20119.56	-2540.441
-75.7	20000.46	-1657.885
-1	19611.41	-445.402
40.05	18952.41	560.8766
81.05	18372.8	1888.834
122.05	18063.14	3422.997
163.1	17832.89	5113.875
122.05	17944.04	4503.509
81.05	18102.84	3818.91
40.05	18221.94	3018.836
-1	18491.89	2210.514
-75.7	18952.41	965.0377
-150.65	19420.86	-486.6429
-225.6	19889.31	-2177.521
-300.05	20389.52	-3909.64
-225.35	20230.72	-3266.281
-150.65	20119.56	-2540.441
-75.7	20000.46	-1690.878
-0.75	19460.55	-288.6865

Table B22. CPLT 69 strain-gauge results for interference-fit plug specimen 2, strain gauges 1 and 4 not working.

Load (kN)	Gauge 2 ($\mu\epsilon$)	Gauge 3 ($\mu\epsilon$)
0	17582.09	401.0993
40.75	17507.9	1440.683
81.55	17178.19	3118.751
122.55	16939.14	4878.677
163.35	16700.1	6794.131
122.55	16823.74	5918.261
81.55	16980.35	4837.749
40.75	17104	3675.379
0	17062.78	2594.867
-74.7	17260.61	1236.041
-149.15	17507.9	40.9285
-223.65	17746.94	-1514.35
-297.85	18068.42	-3356.14
-223.65	18027.2	-2676.72
-149.15	17985.99	-1874.53
-74.45	17903.56	-998.655
0	17664.52	319.2423
40.75	17466.69	1522.54
81.8	17178.19	3200.609
122.55	16897.93	4993.277
163.55	16700.1	6916.916
122.55	16823.74	6000.118
81.55	16939.14	4878.677
40.75	17104	3675.379
0	17062.78	2562.124
-74.7	17219.4	1203.298
-149.15	17425.47	40.9285
-223.65	17705.73	-1481.61
-297.85	18027.2	-3315.21
-223.65	17985.99	-2635.8
-149.15	17903.56	-1833.6
-74.45	17829.37	-957.727
0	17623.3	319.2423

Table B23. CPLT 69 strain-gauge results for interference-fit plug specimen 3, strain gauges 2 and 4 not working.

Load (kN)	Gauge 1 ($\mu\epsilon$)	Gauge 3 ($\mu\epsilon$)
-0.75	-668.176	-2140.58
42	189.8226	-1209.55
84.7	1632.474	230.7684
127.7	3189.019	1862.063
170.65	5155.581	3763.913
127.7	4335.547	3143.225
84.95	3264.948	2442.962
42	2110.827	1551.719
-0.75	1002.263	700.2629
-78.85	-478.353	-700.263
-156.75	-1518.58	-2291.77
-234.6	-2779	-4241.37
-312.5	-4335.55	-6063.64
-234.6	-3705.34	-5403.17
-156.75	-3037.16	-4663.11
-78.6	-2186.76	-3692.3
-0.75	-926.334	-2291.77
42.25	258.1587	-1169.76
84.95	1776.739	310.3438
127.95	3340.877	1862.063
170.65	5003.723	3612.72
127.7	4267.211	2992.032
84.95	3302.913	2251.982
42.25	2224.72	1392.568
-0.75	1184.493	501.3246
-78.85	-220.194	-899.201
-156.75	-1298.39	-2411.13
-234.6	-2634.74	-4122
-312.5	-4259.62	-6023.85
-234.6	-3599.04	-5363.38
-156.75	-2930.86	-4591.5
-78.85	-2110.83	-3652.51
-0.75	-774.476	-2259.94

Table B24. CPLT 69 strain-gauge results for interference-fit plug specimen 4, strain gauges 1 and 4 not working.

Load (kN)	Gauge 2 ($\mu\epsilon$)	Gauge 3 ($\mu\epsilon$)
-0.25	18912.71	74.2337
40.75	18452.2	758.833
81.8	18102.84	2169.273
122.8	17832.89	3662.195
163.8	17634.39	5270.591
122.8	17713.79	4627.232
81.8	17793.19	3860.151
41	17944.04	2895.113
-0.25	18023.44	2012.557
-74.95	18531.6	882.5558
-149.65	18801.55	-362.92
-224.6	19150.9	-1814.6
-299.05	19571.71	-3390
-224.35	19460.55	-2738.4
-149.65	19341.46	-2020.81
-74.95	19230.3	-1212.48
0	18952.41	-123.723
41	18531.6	800.074
82.05	18102.84	2251.755
123.05	17832.89	3744.676
164.05	17634.39	5311.832
123.05	17713.79	4668.473
82.05	17793.19	3901.392
41	17944.04	2936.354
0	18023.44	2053.798
-74.7	18531.6	882.5558
-149.65	18801.55	-362.92
-224.6	19150.9	-1814.6
-299.05	19539.95	-3390
-224.35	19420.86	-2705.41
-149.65	19301.76	-1979.56
-74.7	19190.6	-1171.24

DISTRIBUTION LIST

Fatigue Testing of Mechanical Life Extension Options for Plates Containing Elongated Holes

R.L. Evans and M. Heller

AUSTRALIA

DEFENCE ORGANISATION

Task Sponsor

DGTA

S&T Program

Chief Defence Scientist
FAS Science Policy
AS Science Corporate Management
Director General Science Policy Development
Counsellor Defence Science, London (Doc Data Sheet)
Counsellor Defence Science, Washington (Doc Data Sheet)
Scientific Adviser to MRDC Thailand (Doc Data Sheet)
Scientific Adviser Joint
Navy Scientific Adviser (Doc Data Sheet and distribution list only)
Scientific Adviser - Army (Doc Data Sheet and distribution list only)
Air Force Scientific Adviser
Director Trials

} shared copy

Aeronautical and Maritime Research Laboratory

Director
Chief of Airframes and Engines Division
Research Leader Fracture Mechanics
Research Leader Structural Integrity
Research Leader Aerospace Composites
K Watters
G Clark
K Sharp
K Walker
A Wong
N Goldsmith
P White
I Anderson
M Heller (6 copies)
R Evans (4 copies)

DSTO Library and Archives

Library Fishermans Bend (Doc Data Sheet)
Library Maribyrnong (Doc Data Sheet)
Library Salisbury
Australian Archives
Library, MOD, Pymont (Doc Data sheet)
US Defense Technical Information Center (2 copies)
UK Defence Research Information Centre (2 copies)
Canada Defence Scientific Information Service
NZ Defence Information Centre
National Library of Australia

Capability Systems Staff

Director General Maritime Development (Doc Data Sheet)
Director General Aerospace Development

Knowledge Staff

Director General Command, Control, Communications and Computers (DGC4)
(Doc Data Sheet)

Army

ABCA Standardisation Officer, Tobruk Barracks, Puckapunyal 3662 (4 copies)
SO (Science), DJFHQ(L), MILPO Gallipoli Barracks, Enoggera QLD 4051 (Doc
Data Sheet)

Air Force

CENG 501 Wing, Amberley
OIC ATF ATS, RAAFSTT, WAGGA

Intelligence Program

DGSTA Defence Intelligence Organisation
Manager, Information Centre, Defence Intelligence Organisation

Corporate Support Program

Library Manager, DLS-Canberra

UNIVERSITIES AND COLLEGES

Australian Defence Force Academy
Library
Head of Aerospace and Mechanical Engineering
Serials Section (M list), Deakin University Library, Geelong 3217
Hargrave Library, Monash University (Doc Data Sheet)
Librarian, Flinders University

OTHER ORGANISATIONS

NASA (Canberra)
AusInfo

OUTSIDE AUSTRALIA**ABSTRACTING AND INFORMATION ORGANISATIONS**

Library, Chemical Abstracts Reference Service
Engineering Societies Library, US
Materials Information, Cambridge Scientific Abstracts, US
Documents Librarian, The Center for Research Libraries, US

INFORMATION EXCHANGE AGREEMENT PARTNERS

Acquisitions Unit, Science Reference and Information Service, UK
Library - Exchange Desk, National Institute of Standards and Technology, US
National Aerospace Laboratory, Japan
National Aerospace Laboratory, Netherlands
SPARES (5 copies)

Total number of copies: 66

DEFENCE SCIENCE AND TECHNOLOGY ORGANISATION DOCUMENT CONTROL DATA				1. PRIVACY MARKING/CAVEAT (OF DOCUMENT)	
2. TITLE Static and Fatigue Testing of Mechanical Life Extension Options for Plates Containing Elongated Holes			3. SECURITY CLASSIFICATION (FOR UNCLASSIFIED REPORTS THAT ARE LIMITED RELEASE USE (L) NEXT TO DOCUMENT CLASSIFICATION) Document (U) Title (U) Abstract (U)		
4. AUTHOR(S) R. L. Evans and M. Heller			5. CORPORATE AUTHOR Aeronautical and Maritime Research Laboratory 506 Lorimer St Fishermans Bend Vic 3207 Australia		
6a. DSTO NUMBER DSTO-TR-1202		6b. AR NUMBER AR-012-007		6c. TYPE OF REPORT Technical Report	7. DOCUMENT DATE August 2001
8. FILE NUMBER M1/9/610		9. TASK NUMBER AIR 98/220	10. TASK SPONSOR DGTA	11. NO. OF PAGES 62	12. NO. OF REFERENCES 19
13. URL on the World Wide Web http://www.dsto.defence.gov.au/corporate/reports/DSTO-TR-1202.pdf				14. RELEASE AUTHORITY Chief, Airframes and Engines Division	
15. SECONDARY RELEASE STATEMENT OF THIS DOCUMENT <i>Approved for public release</i> OVERSEAS ENQUIRIES OUTSIDE STATED LIMITATIONS SHOULD BE REFERRED THROUGH DOCUMENT EXCHANGE, PO BOX 1500, SALISBURY, SA 5108					
16. DELIBERATE ANNOUNCEMENT No Limitations					
17. CASUAL ANNOUNCEMENT Yes					
18. DEFTEST DESCRIPTORS Fatigue life; F-111C wing pivot fittings; Holes (openings); Cold working; Interference fit devices; Expansion					
19. ABSTRACT F-111 representative static and fatigue testing has been undertaken to assess the suitability of AMRL designed stress-bridge and interference-fit plug options for the fatigue life enhancement of plates containing non-circular elongated holes of 2:1 aspect ratio. For the stress-bridge design, an improvement in strain concentration factor of 38% was demonstrated for lower magnitude remote loads as compared to plates with unenhanced holes. Conversely, during typical high loads, the alternating strain range was negligibly improved due to slipping of the feet. Hence during the fatigue tests there was extensive specimen cracking. However, excellent results were achieved with the interference-fit plug design, where the peak elastic strain concentration factor was reduced by 79% as compared to the unenhanced case. This design also prevented the introduction of detrimental residual tensile stresses during high loads. Consequently, for these enhanced specimens, crack growth during fatigue testing was completely prevented, and very large extensions in fatigue lives were demonstrated. Thus the interference-fit plug is considered a very suitable option for the fatigue life extension of elongated holes such as the critical fuel flow vent holes in the F-111 wing pivot fitting.					

